Cambrian-1: A Fully Open, *Vision-Centric* Exploration of Multimodal LLMs

Shengbang Tong*, Ellis Brown*, Penghao Wu*, Sanghyun Woo, Manoj Middepogu, Sai Charitha Akula, Jihan Yang, Shusheng Yang, Adithya Iyer, Xichen Pan, Austin Wang, Rob Fergus, Yann LeCun, Saining Xie†

New York University

Abstract

We introduce Cambrian-1, a family of multimodal LLMs (MLLMs) designed with a vision-centric approach. While stronger language models can enhance multimodal capabilities, the design choices for vision components are often insufficiently explored and disconnected from visual representation learning research. This gap hinders accurate sensory grounding in real-world scenarios. Our study uses LLMs and visual instruction tuning as an interface to evaluate various visual representations, offering new insights into different models and architectures—self-supervised, strongly supervised, or combinations thereof—based on experiments with over 20 vision encoders. We critically examine existing MLLM benchmarks, addressing the difficulties involved in consolidating and interpreting results from various tasks, and introduce a new vision-centric benchmark, CV-Bench. To further improve visual grounding, we propose the Spatial Vision Aggregator (SVA), a dynamic and spatially-aware connector that integrates high-resolution vision features with LLMs while reducing the number of tokens. Additionally, we discuss the curation of high-quality visual instruction-tuning data from publicly available sources, emphasizing the importance of data source balancing and distribution ratio. Collectively, Cambrian-1 not only achieves state-of-the-art performance but also serves as a comprehensive, open cookbook for instruction-tuned MLLMs. We provide model weights, code, supporting tools, datasets, and detailed instruction-tuning and evaluation recipes. We hope our release will inspire and accelerate advancements in multimodal systems and visual representation learning.

🌐	**Website**	https://cambrian-mllm.github.io
	Code	https://github.com/cambrian-mllm/cambrian
🤗	**Models**	https://huggingface.co/nyu-visionx/
🤗	**Data**	https://huggingface.co/datasets/nyu-visionx/Cambrian-10M
🤗	**CV-Bench**	https://huggingface.co/datasets/nyu-visionx/CV-Bench
	Evaluation	https://github.com/cambrian-mllm/cambrian

*Project Lead

†Corresponding Author

Contents

1 Introduction **3**

2 Multimodal LLMs: Preliminaries and Related Work **4**

3 Evaluating Visual Representations through MLLMs **6**
3.1 Analyzing the Benchmarks 6
3.2 Cambrian Vision-Centric Benchmark (CV-Bench) 7
3.3 Instruction Tuning Recipes 8
3.4 MLLMs as a Visual Representation Evaluator 10
3.5 Combining Multiple Vision Encoders 12

4 Spatial Vision Aggregator (SVA): A New Connector Design **12**

5 Instruction Tuning Data for Training MLLMs **15**
5.1 Data Collection 15
5.2 Data Curation 16
5.3 Alleviating the "Answer Machine Phenomenon" via System Prompts 17

6 State of the Art Performance **18**

7 Discussion **19**

References **22**

A Training, Infrastructure, and Implementation **29**

B Analyzing the Benchmarks **29**

C Cambrian Vision-Centric Benchmark (CV-Bench) **29**
C.1 Curation Procedure 29
C.2 Human verification 30
C.3 Benchmark Evaluation 30

D Vision Models in MLLMs **31**
D.1 Details of Vision Models 31
D.2 Full Results of Different Vision Backbone in MLLM 31
D.3 Model Ensemble 33

E Data **34**
E.1 Catalog of Visual Instruction Data 34
E.2 Additional System Prompts used in Cambrian Data 34
E.3 Data Engine 34
E.4 Full results on data curation experiment 39
E.5 737K and 5M Mixes 39

F Implementation Details **39**

G Evaluation Details **39**
G.1 System Prompts Used in Evaluation 39
G.2 Ablation Study on Fuzzy Matching Vs LLM Judgement 40

1. Introduction

There is a long-standing debate in philosophy about whether understanding and meaning in language require sensory grounding. Aristotle's emphasis on acquiring knowledge through sensory experience and empirical observation was central to his ancient Peripatetic school and remains influential to this day [7]; Aquinas famously formalized these ideas in the 13th century with the Peripatetic axiom: "*Nihil est in intellectu quod non sit prius in sensu*" (Nothing is in the intellect that was not first in the senses) [6]. Though many philosophers disagree [18], it is evident that having robust and highly capable sensory grounding is at least beneficial. Consider the *Cambrian explosion*, during which the emergence of vision is believed [98] to have been crucial for early animals to not only find food and avoid predators but also to evolve and improve. In fact, most human knowledge (and nearly all animal knowledge) is acquired through sensory experiences like sight, hearing, touch, taste, and smell, through interactions with the physical world [100]. These sensory experiences are fundamental to understanding the world around us and are crucial for real-world actions and decision-making.

Beyond philosophical debates, recent advances in multimodal large language models (MLLMs) have brought the topic of *visual representation learning vs. language understanding* into practical focus. Language models have shown strong scaling behaviors [48], and recent advancements in multimodal learning are largely driven by the development of better, larger LLMs [74]. On the other hand, the design choices for vision components are often insufficiently explored and *disconnected* from visual representation learning research. For instance, many pioneering frameworks such as LLaVA [75] use vision transformer-based CLIP models [102, 136], which are strongly supervised by language[1], as the vision feature extractor. While other visual representations, such as self-supervised DINO [96], are being explored [117], there is a lack of comprehensive and systematic study in this domain. This gap exists primarily because such studies are challenging: MLLMs involve a complex training and evaluation pipeline with numerous design decisions to consider. In this work, we aim to bridge the gap by exploring MLLMs from a vision-centric perspective. More specifically, we use MLLM instruction tuning as an evaluation protocol for various visual representations (illustrated in Fig. 1).

Our motivation for this study also stems from two potential concerns of the current multimodal learning research: 1) relying too heavily too early on language can act as a shortcut [40, 135], compensating for the deficiencies in learning effective visual representations, and 2) existing benchmarks may not provide adequate guidance for real-world scenarios—where visual grounding is crucial for robust multimodal understanding. These concerns are not unfounded, as researchers have started to notice that visual grounding is becoming a bottleneck for applying MLLMs in some challenging real-world applications, despite significant progress in improving general capabilities [35, 117, 127].

From another perspective, traditional evaluation protocols for visual representation learning (e.g., *linear probing* and *end-to-end fine-tuning* on datasets like ImageNet-1K [105], COCO [72], and ADE20K [145]) are becoming saturated and do not reflect the diverse perception challenges found in real-world distributions. On the other hand, using language in the form of visual question answering (VQA) offers a flexible and robust evaluation protocol. Our study aims to explore this new protocol design, setting it up to gain insights that will guide the development of better visual representations in the future. Furthermore, to better evaluate visual representations in this integrated setting, we develop a vision-centric MLLM benchmark, CV-Bench, by transforming traditional vision benchmarks into VQA format (Section 3.2).

[1] We emphasize that CLIP training should be considered as *strongly supervised*, as language provides significantly richer supervision than class labels.

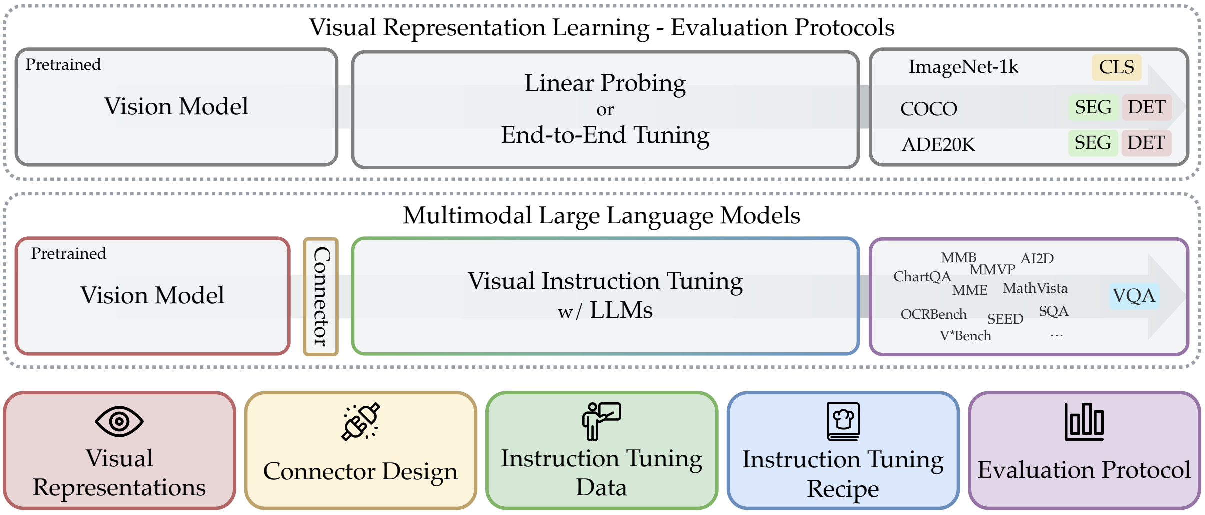

Figure 1 | We draw parallels between traditional protocols and the use of MLLMs for evaluating visual representations. MLLMs employ visual question answering to address a diverse array of real-world perception tasks. The bottom section highlights the five key pillars studied in Cambrian-1.

Cambrian-1 is structured around five key pillars, each offering important insights into the design space of MLLMs:

- **Visual Representations**: We explore various vision encoders and their combinations. §3.4
- **Connector Design**: We design a new dynamic and spatially-aware connector that integrates vision features with LLMs while reducing the number of tokens. §4
- **Instruction Tuning Data**: We curate high-quality visual instruction-tuning data from public sources, emphasizing the importance of distribution balancing. §5
- **Instruction Tuning Recipes**: We discuss instruction tuning strategies and practices. §3.3
- **Benchmarking**: We analyze existing MLLM benchmarks, cluster them into 4 intuitive groups, and introduce a new vision-centric benchmark "CV-Bench". §3.1, §3.2

As a by-product of our exploration, Cambrian-1 introduces a family of state-of-the-art MLLMs that achieve top performance across diverse benchmarks and excel in visual-centric tasks (Section 6). We provide model weights, open-source code, datasets, and detailed recipes for model training and evaluation. We hope our work will strengthen the open research community and accelerate research in both visual representation learning and multimodal systems.

2. Multimodal LLMs: Preliminaries and Related Work

The key components of MLLM research include the *Large Language Model*, *Visual Encoder*, *Multimodal Connector*, *Data Curation Pipeline*, *Instruction Tuning Strategy*, and *Evaluation & Benchmarking*. Each component has its intricacies, and understanding their interactions presents significant challenges. Our study investigates these aspects from a vision-centric perspective.

Large Language Model Advanced LLMs [3, 94, 118, 119] are the foundation of an MLLM. After instruction-tuning on multimodal data, these models can be prompted to solve a variety of complex tasks and generate free-form responses leveraging input from a visual encoder. Recent MLLM research focuses on enhancing the LLM backbone [9, 68, 74], resulting in improved performance on benchmarks like MMMU [134] and AI2D [47]. However, this improvement raises the concern that our current *multimodal* evaluation is biased by the development of LLMs, neglecting a true assessment of visual perception. For example, some benchmarks such as

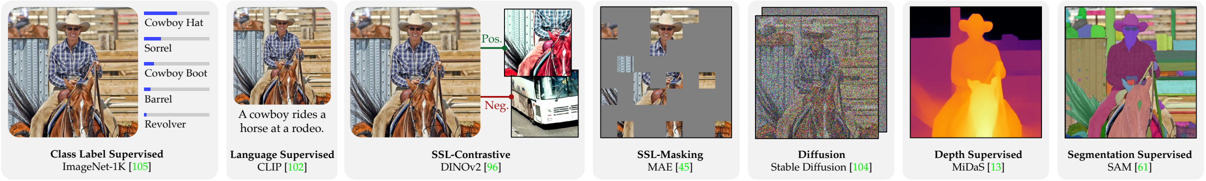

Figure 2 | Examples of various vision models, objectives, and architectures studied. Image from [41].

MMMU [134] are dominated by LLM capabilities, underscoring the need for evaluations that genuinely assess multimodality (see Section 3.1).

Visual Encoder Most MLLMs utilize language-supervised models like CLIP [102, 113, 136], which benefit from the massive scale of noisy web image-text data. However, there is a much broader pool of visual models that learn representations using only visual signals—such as self-supervised models [8, 96], segmentation [61], depth-supervised [67], and diffusion models [104] (see Fig. 2). Recent work [80, 117] advocates for incorporating these diverse vision models into MLLMs. In this study, we systematically examine the impact of various vision backbones on MLLM performance (Section 2) and explore the benefits of model ensembles (Section 3.5).

Multimodal Connector Representations from a visual encoder cannot be natively processed by an LLM—they must be mapped into the LLM token space by a *connector*. There are three primary approaches to connector design: Resamplers [5], Q-Formers [10, 31], and MLP Projectors [73, 75]. We begin our exploration using an MLP projector, which is highly effective but presents challenges: the visual token count grows quadratically with image resolution, inhibiting scaling context length input resolution. For example, LLaVA-Next [74] requires 2880 visual tokens to process one 672px image. To address this, we explore new vision connector designs that process high-resolution images while maintaining a smaller number of visual tokens (Section 4).

Instruction Tuning Data Visual instruction tuning data is crucial but hard to collect, as it rarely naturally exists on the internet. Previous work [31, 73, 91] transforms existing VQA benchmarks [43, 62] into instruction tuning data, showing marked MLLM performance improvements. With this inspiration, we collect all VQA benchmarks and visual interaction data that we can find (Fig. 9), study data balancing and category mixtures (Section 5.2), and develop an internet data collection engine to fill in the gaps (Section 5.1).

Instruction Tuning Most current MLLMs leverage pre-trained LLMs and visual encoders, fine-tuning the LLM and connector using visual instruction tuning data. Some aspects of the tuning recipe are up for debate, including whether to pre-train the connector before joint fine-tuning with the LLM , and whether to freeze or unfreeze the vision encoder during fine-tuning [56, 91]. Additionally, some recent proprietary models explore end-to-end training from scratch [42, 95]. In this work, we use pre-trained models and revisit the debated recipe aspects with extensive studies, providing more insights for future MLLM research (Section 3.3).

Evaluation & Benchmarking There is an extensive set of benchmarks that evaluate various aspects of MLLMs, such as perception [39, 76], knowledge [84, 85], chart interpretation [77, 89], and visual capabilities [117, 127]. Instead of over-optimizing for specific benchmarks, we advocate for examining aggregates of benchmarks that focus on specific capabilities. To achieve this, we analyze existing benchmarks, categorize them, and assess the extent to which they measure *multimodality* (Section 3.1). Additionally, we find there are currently few benchmarks focused on vision-centric evaluation, and those that do exist contain relatively few images, leading to higher variance during evaluation. To address this issue, we propose a new vision-centric benchmark by reformulating classic vision tasks (Section 3.2).

3. Evaluating Visual Representations through MLLMs

Current MLLMs predominantly rely on CLIP [102] as the visual encoder due to its pre-alignment with language and ease of adaptation to the LLM token space. However, strong language priors can be a double-edged sword—they compensate for deficiencies in learning effective visual representations [117] and diminish insights gained from extensive visual representation learning research. In this section, we systematically evaluate how various visual encoder choices (see Fig. 2) impact the multimodal capabilities of MLLMs. We also advocate for using MLLM evaluation as a robust framework for assessing visual representation methods, moving beyond traditional protocols like linear probing and end-to-end fine-tuning to more faithfully reflect the diverse perception challenges in real-world scenarios and to better guide the development of improved visual representations. Specifically, in this section we:

§3.1. Analyze the Benchmarks
§3.2. Introduce CV-Bench
§3.3. Study Instruction Tuning Recipes
§3.4. Use MLLMs as a Visual Representation Evaluator
§3.5. Investigate Combining Multiple Vision Encoders

3.1. Analyzing the Benchmarks

To effectively evaluate visual representations and MLLMs, we first need to select benchmarks that accurately assess the *multimodal* capabilities of these models. We use a suite of commonly used benchmarks [19, 39, 47, 50, 76, 77, 84, 85, 89, 112, 117, 128, 134], which is the intersection of those used in recent MLLM research [68, 70, 128]. To help interpret our results, we begin by analyzing the benchmarks themselves. Here, we train MLLMs with 23 different vision backbones (see Table 9) from a variety of model families (see Fig. 2) using a 2-stage instruction tuning process initially proposed in [75]: first training connector on 1.2M adapter data from ShareGPT-4V [22] followed by fine-tuning both the connector and LLM on 737K instruction tuning data (see more details in Appendices E.5 and F). Full benchmark results in Table 10.

Who's answering the question: the LLM or MLLM? Determining whether a benchmark *truly* needs visual input to be solved has been a persistent challenge in vision-language research [2, 21, 43, 87]. In this study, we compare the performance of MLLMs with and without visual input[2], and also calculate the expected score via randomly guessing. These three conditions

[2] We note that our instruction-tuning data includes text-only data, so text-only questions are not OOD.

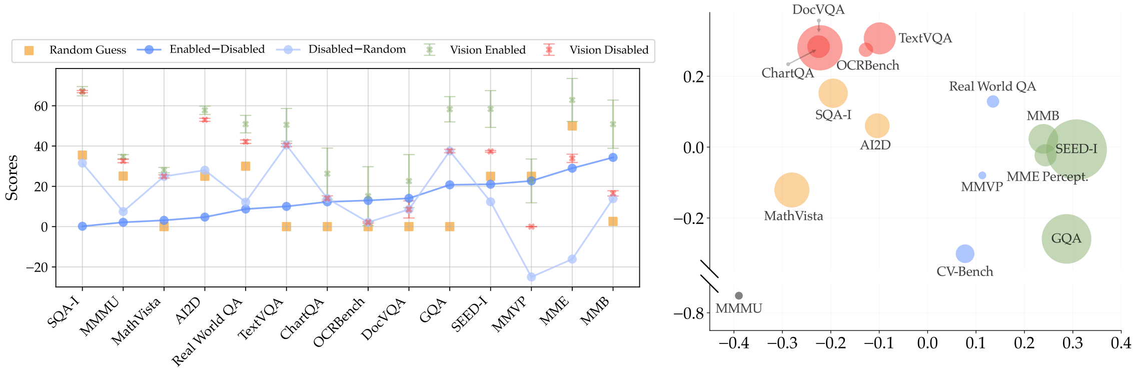

Figure 3 | **Left:** Performance comparison of MLLMs with visual input enabled and disabled across various benchmarks. Benchmarks are sorted by the difference between the average score with vision enabled and disabled. **Right:** Principal component analysis displaying clusters of benchmarks based on performance metrics, with bubble size corresponding to benchmark size. We label the clusters as "General" in green, "Knowledge" in yellow, "Chart & OCR" in red, and "Vision-Centric" in blue.

are visualized in Fig. 3-left, with benchmarks sorted by the difference between the average score with vision enabled and disabled. SQA-I[3], MMMU, MathVista, and AI2D display less than a 5% gap between vision enabled and disabled, suggesting that these benchmarks may not significantly depend on visual input and rather heavily rely on the base LLM. TextVQA and GQA both demonstrate a nearly 40% positive gap between random guessing and vision-disabled scores, implying a strong language bias in these benchmarks. On the other hand, the vision-disabled performance on benchmarks like MMVP and MME Perception is notably worse than random guessing, suggesting that strong visual grounding is particularly crucial.

Clustering the Benchmarks To better understand the different aspects of MLLM performance, we analyze the correlations between the performance of our 23 MLLMs on each benchmark. A confusion matrix (Fig. 15) reveals that certain benchmarks, such as MMMU, are largely uncorrelated with the others. We perform principal component analysis on the benchmark scores and observe the formation of clusters corresponding to "General," "Knowledge," "Chart & OCR," and "Vision-Centric" categories (Fig. 3-right). We assign MMMU to the knowledge category based on the types of questions it includes (see Appendix B). We also find that existing vision-centric benchmarks [117, 128] are of insufficient size (see Fig. 3-right), challenging the robustness of evaluating such capabilities. Furthermore, these benchmarks do not cover crucial visual elements such as depth and spatial awareness.

Finding 1: Most benchmarks do not properly measure vision-centric capabilities, and the ones that do have very few samples.

3.2. Cambrian Vision-Centric Benchmark (CV-Bench)

To address the limitations of existing vision-centric benchmarks, we introduce the Cambrian Vision-Centric Benchmark (CV-Bench). With **2638 manually-inspected examples**, CV-Bench provides significantly more examples than other vision-centric MLLM benchmarks—3.5× more than RealWorldQA [128] and 8.8× more than MMVP [117]. By repurposing standard vision benchmarks [16, 72, 145], we can assess models at classic vision tasks within a multimodal context. Leveraging the rich ground truth annotations from the benchmarks, we formulate natural language questions that probe the fundamental 2D and 3D understanding of the models.

As visualized in Fig. 4 and detailed in Table 1, CV-Bench evaluates 2D understanding via spatial relationships & object counting, and 3D understanding via depth order & relative distance.

CV-Bench Curation Below we describe the procedure for programmatically constructing questions for each task. To ensure reliability, we also *manually inspect each question*, removing those that are unclear, ambiguous, or erroneous. See Appendix C for details.

Spatial Relationship (2D). We consider images with two distinct ground-truth object categories and use visual prompts (bounding boxes) to avoid ambiguity when multiple instances are present. In these questions, we designate an anchor object, and the question asks for the direction of the other object relative to this anchor.

Object Counting (2D). This tests the model's ability to count objects. When generating options for these questions, we construct multiple-choice options that are similar to the correct answer. For example, if the correct answer is 4, the options might be 2, 3, 4, 5, & 6. We also include existence check examples where the correct count is 0.

Depth Order (3D). We consider images with two distinct categories (i.e., object A and object B) and use visual prompts (e.g., bounding boxes with two different colors) to avoid ambiguity.

[3] The subset of SQA [84] with images.

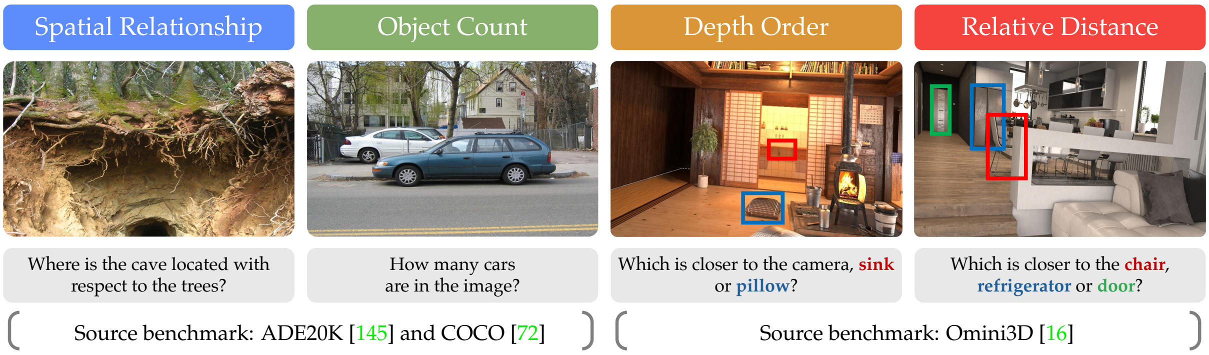
Spatial Relationship
Object Count
Depth Order
Relative Distance
Where is the cave located with respect to the trees?
How many cars are in the image?
Which is closer to the camera, sink or pillow?
Which is closer to the chair, refrigerator or door?
Source benchmark: ADE20K [145] and COCO [72]
Source benchmark: Omini3D [16]

Figure 4 | **Cambrian Vision-Centric Benchmark (CV-Bench).** We repurpose standard vision benchmarks to evaluate the fundamental 2D and 3D visual understanding of MLLMs. See Section 3.2 for more details.

Type	Task	Description	Sources	# Samples
2D	**Spatial Relationship**	Determine the relative position of an object w.r.t. the anchor object. Consider left-right or top-bottom relationship.	ADE20K COCO	650
	Object Count	Determine the number of instances present in the image.	ADE20K COCO	788
3D	**Depth Order**	Determine which of the two distinct objects is closer to the camera.	Omni3D	600
	Relative Distance	Determine which of the two distinct objects is closer to the anchor object.	Omni3D	600

Table 1 | Breakdown of the 2D and 3D tasks evaluated in the Cambrian Vision-Centric Benchmark (CV-Bench). The examples are sourced from ADE20K [145], COCO [72], and Omni3D [16].

We define "closer" as follows: object A is closer to the camera than object B only if the farthest vertex of object A is closer[4] to the camera than the nearest vertex of object B by a specified offset.

Relative Distance (3D). We consider images with three distinct categories (i.e., anchor, object A, and object B), and use visual prompts (e.g., bounding boxes with three different colors) to avoid ambiguity. Object A is closer than object B only if the farthest distance from A's vertices is shorter than the shortest distance from B's vertices to the anchor object by a certain offset.

Finding 2: Existing vision benchmarks can be effectively repurposed into VQA questions, enabling the assessment of vision-centric MLLM capabilities.

3.3. Instruction Tuning Recipes

MLLMs start with pre-trained LLM and vision backbones, connecting these modules with a connector such as a projector (MLP). The original LLaVA [73, 75] proposes a 2-stage frozen training process: first, pre-training a connector between frozen LLM and vision backbones using adapter data (such as VQA based on captions), and then fine-tuning both the connector and LLM with instruction tuning data while leaving the vision encoder frozen. Various studies [22, 56, 74, 91] have drawn different conclusions regarding the optimal training methodology for MLLMs. Here, we revisit this topic with extensive experiments.

For our experiments, we tune a set of MLLMs using Vicuna-1.5-7B as the LLM backbone and each of our 23 vision models (Table 9) as the visual encoder. We use a 737K instruction tuning data mix for all experiments here (see Appendix F). All hyperparameters are matched across each experimental setting—highlighting the impact of different tuning strategies with each visual encoder. All experimental settings and results are tabulated in Appendix D.2.

[4] We use the Euclidean distance.

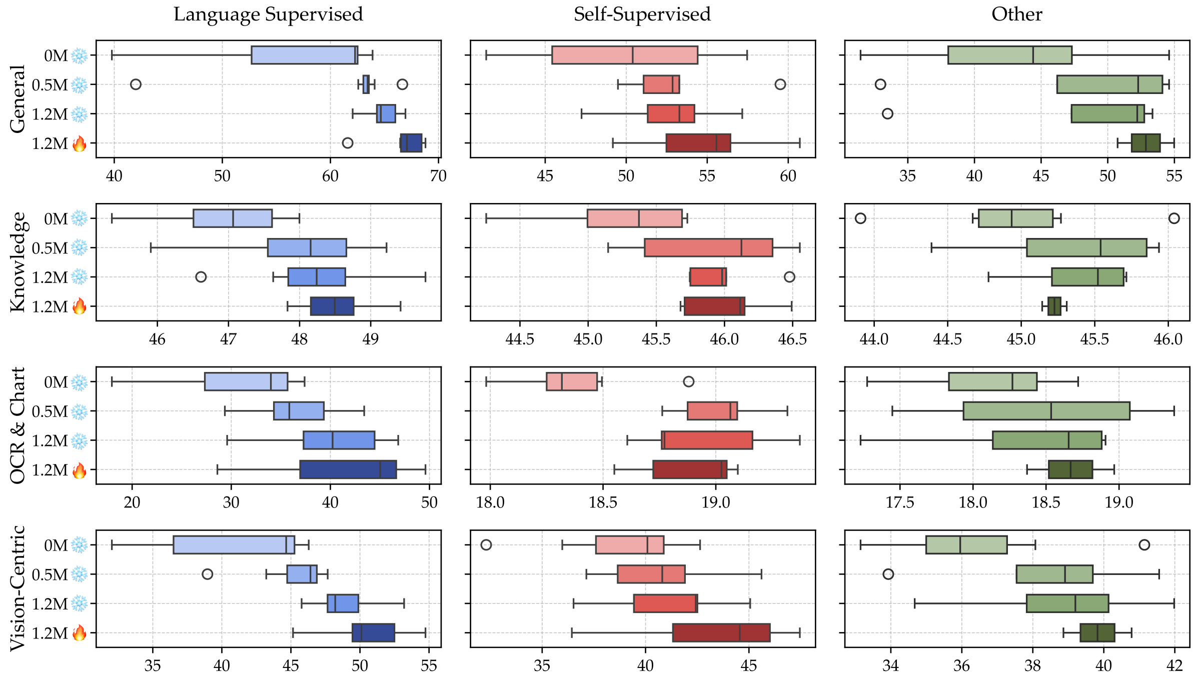

Figure 5 | **Effect of Training Recipe on Model Performance**. Boxplots display the distribution of benchmark scores across benchmark categories for different training recipes and types of visual encoders (Language-Supervised, Self-Supervised, and Other). The four training recipes include freezing the visual encoder with various amounts of adapter data (0M❄️, 0.5M❄️, 1.2M❄️) as well as unfreezing it with 1.2M🔥 adapter data. **Amount of Adapter Data**: All model types show increased performance on general and vision-centric benchmarks with more adapter data; knowledge benchmarks show mixed results; OCR & chart benchmarks benefit from more data for language-supervised models. **Unfreezing**: Unfreezing the visual encoder with 1.2M🔥 adapter data generally benefits all categories. Language-supervised models benefit from unfreezing across the board; self-supervised models benefit particularly well in vision-centric benchmarks but continue to struggle in OCR.

One Stage vs Two Stage Training Recent work [56] advocates for skipping connector pre-training, claiming this "*reduces compute cost without harming downstream performance*." To explore whether this claim holds—especially when using non-language-supervised visual encoders—we conduct experiments using 0, 0.5M, and 1.2M adapter data. Following LLaVA's recipe [75], we tune only the connector on the adapter data during this first phase, before unfreezing the LLM and connector during instruction tuning on the 737K mix. Fig. 5 shows that pre-training the connector first enhances model performance and that more adapter data further improves performance across all domains. Thus, we subsequently adopt 2-stage training with 1.2M adapter data as our standard setup.

Finding 3: Two-stage training is beneficial; more adapter data further improves results.

Freeze vs Unfreeze Vision Encoder There are also mixed practices in freezing [56, 73, 75] or unfreezing [38, 74] vision backbones during fine-tuning. Some argue that unfreezing the vision backbone significantly degrades performance [56]. Our experiments demonstrate that unfreezing benefits performance across all benchmarks except for a marginal change in knowledge benchmarks (Fig. 5). We suspect this is due to the composition of the 737K instruction tuning data and the LLM-heavy focus of these benchmarks (see Section 3.1). We note that unfreezing the vision backbone introduces additional computational overhead, which prohibits testing on some larger vision models under current sharding strategies (see more details in Appendix F).

Finding 4: Unfreezing the vision encoder is widely beneficial. Language-supervised models always benefit; SSL models particularly benefit on vision-centric benchmarks.

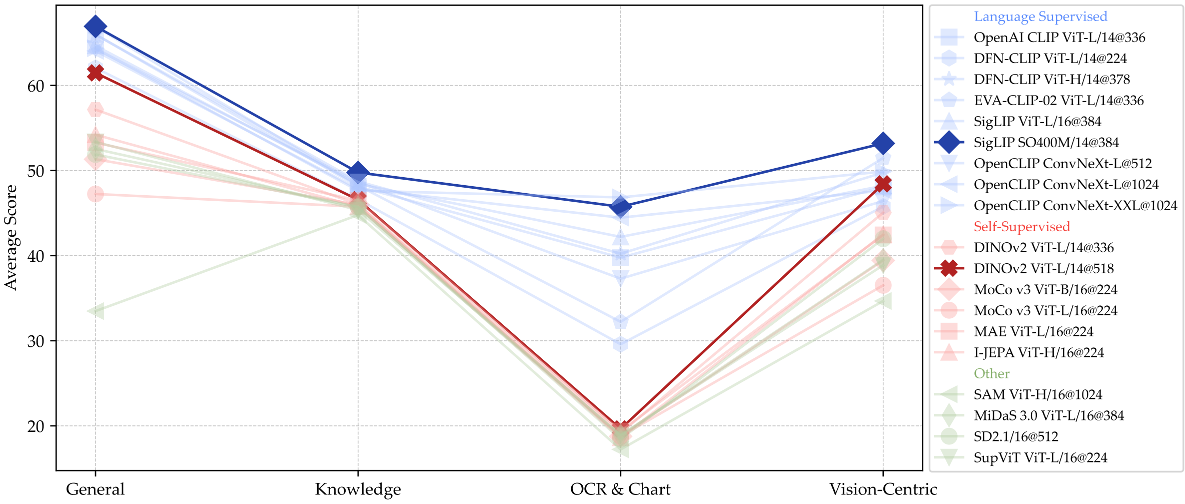

Figure 6 | **Evaluating Visual Representations with MLLMs** While language-supervised models outperform self-supervised or other models, a well-trained self-supervised model like DINOv2 can also achieve competitive performance on vision-centric tasks.

Language Supervised							**Self-Supervised & Other**						
Model	Architecture	All	G	K	O	V	Model	Architecture	All	G	K	O	V
SigLIP	ViT-SO400M/14@384	1	1	1	2	1	DINOv2	ViT-L/14@518	1	1	1	1	1
OpenCLIP	ConvNeXt-XXL@1024	2	6	8	1	3	DINOv2	ViT-L/14@336	2	2	3	3	2
DFN-CLIP	ViT-H/14@378	3	4	2	5	4	MAE	ViT-L/16@224	3	5	2	2	4
OpenCLIP	ConvNeXt-L@1024	4	8	7	3	8	I-JEPA	ViT-H/14@224	4	3	6	8	3
SigLIP	ViT-L/16@384	5	5	4	4	6	SD2.1	VAE+UNet/16@512	5	7	9	9	5
OpenAI CLIP	ViT-L/14@336	6	3	6	6	7	MiDaS 3.0	ViT-L/16@384	6	6	8	5	6
EVA-CLIP-02	ViT-L/14@336	7	2	5	8	2	SupViT	ViT-L/16@224	7	4	9	4	8
OpenCLIP	ConvNeXt-L@512	8	7	3	7	9	MoCo v3	ViT-B/16@224	8	8	4	7	7
DFN-CLIP	ViT-L/14@224	9	9	9	9	10	MoCo v3	ViT-L/16@224	9	9	5	6	9
DINOv2*	ViT-L/14@518	10	10	10	10	5	SAM	ViT-H/16@1024	10	10	10	10	10

Table 2 | Benchmark performance rankings for MLLMs built upon language-supervised and self-supervised vision encoders across all benchmarks (All), and across general (G), knowledge (K), OCR & chart (O), and vision-centric (V) benchmark categories. Full results for all models on each benchmark are tabulated in Table 12. *We add DINOv2 here to show its standing amongst the CLIP models.

3.4. MLLMs as a Visual Representation Evaluator

As discussed in earlier sections, MLLMs provide a new interface to explore aspects of vision models beyond traditional benchmarks like ImageNet-1k linear probing. We study the 2-stage instruction tuning setting using 1.2M adapter data, 737K fine-tuning data, and frozen visual encoders to allow comparison of the widest range of models.

We evaluate on benchmarks detailed in Section 3.1, calculating the average performance[5] for each category and visualize the results in Fig. 6 (full results in Appendix D). Our findings highlight the advantages of language-supervised models over non-CLIP models across all benchmark categories, with significantly better performance on chart and OCR-related benchmarks. We hypothesize that this is due to CLIP's *training data*, such as LAION [107], containing abundant OCR and text-heavy data, whereas SSL and other vision models primarily train on natural images with significantly less text content. It is also noteworthy that language-supervised models are typically trained with a very large pool of data, ranging from 400 million [102] to 10 billion [23] samples, whereas the largest vision self-supervised training dataset, like DINOv2,

[5] Before averaging, we divide the MME Perception score by 20 to have the same scale as other benchmarks.

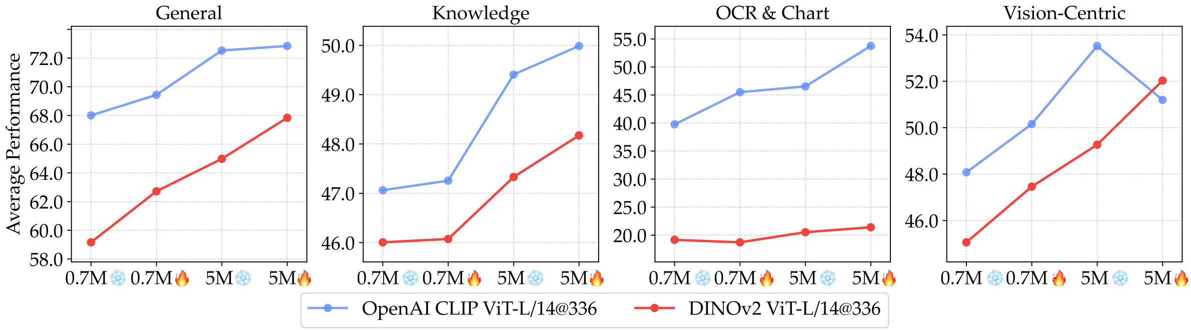

Figure 7 | **Continued Fine-Tuning Narrows the Gap Between CLIP and DINOv2**. The average performance of MLLMs built upon OpenAI CLIP ViT-L/14@336 and DINOv2 ViT-L/14@336 encoders are visualized across benchmark categories. Performance is compared with 0.7M and 5M instruction tuning data in both frozen (❄️) and unfrozen (🔥) settings. DINOv2 shows significant performance improvement with increased data and unfreezing—surpassing the 0.7M❄️ CLIP model in several benchmarks and narrowing and bridging the gap to the 5M🔥 model in knowledge and vision-centric tasks, respectively.

consists of only *142 million samples* [96].

The performance comparison in Fig. 6 between DINOv2, other SSL models, and language-supervised models underscores the potential for training superior vision-only models with more data and improved techniques. Additionally, we observe that higher-resolution models particularly enhance performance on chart and vision-centric benchmarks while remaining neutral on general VQA and knowledge-based VQAs. While the majority of the backbones we examine are ViT-based [33], **ConvNet-based architectures** (such as OpenCLIP ConvNeXt [79]) are inherently well-suited for high-resolution image processing [121] and can produce superior results on OCR & Chart and Vision-Centric benchmarks. In vision-centric benchmarks, the gap between language-supervised and other types of vision models is smaller, with a well-trained self-supervised DINOv2 model even outperforming some language-supervised models.

> ***Finding 5:*** High-res encoders greatly enhance performance on chart & vision-centric benchmarks, and ConvNet-based architectures are inherently well-suited for such tasks.

Narrowing the gap between Language- and Self-Supervised models Above, we observe that DINOv2 stands midway between self-supervised models and language-supervised models on general and knowledge benchmarks, even outperforming some language-supervised models on vision-centric benchmarks at a higher resolution. Here, we study whether the continued finetuning of an MLLM based on a self-supervised model can achieve performance similar to that of a language-supervised model. Given that DINOv2 is trained with much less data compared to CLIP, we investigate increasing the amount of visual fine-tuning data while unfreezing the vision backbones to bridge this gap. Specifically, we scale up the instruction tuning data from 737K to 5M (see more details in Appendix E.5), and instruction tune MLLMs with DINOv2 ViT-L/14@336 and OpenAI CLIP ViT-L/14@336 encoders in both frozen and unfrozen settings. In Fig. 7, we observe that by unfreezing the vision backbone, the DINOv2-based MLLM fine-tuned with 5M data surpasses the MLLM trained with a CLIP model on 0.7M data. Additionally, the gap between DINOv2 and the CLIP models is reduced under the 5M setting.

> ***Finding 6:*** Language supervision offers strong advantages, but the performance gap can be narrowed with SSL methods given enough data and proper tuning.

Vision Backbone		General				Knowledge				OCR & Chart				Vision-Centric			
Method	Average	MME^{P}	MMB	SEED^{I}	GQA	SQA^{I}	MMMU^{V}	$\text{MathVista}^{\text{M}}$	AI2D	ChartQA	OCRBench	TextVQA	DocVQA	MMVP	RealWorldQA	$\text{CV-Bench}^{\text{2D}}$	$\text{CV-Bench}^{\text{3D}}$
SigLIP+DINOv2	51.61	1,432.02	61.28	65.99	63.30	68.82	35.69	29.40	60.01	43.00	35.70	60.40	37.54	30.00	53.99	55.52	53.58
SigLIP+DINOv2+ConvNext	54.52	1,503.51	63.83	67.97	63.95	70.40	35.99	29.30	60.69	48.20	36.90	64.97	45.53	34.67	58.69	55.74	60.33
SigLIP+DINOv2+ConvNext+CLIP	54.74	1,479.46	63.32	67.63	64.04	71.39	35.49	29.10	59.88	50.24	39.60	64.55	46.12	32.67	58.95	58.54	60.42
SigLIP+ConvNext	54.53	1,494.97	64.60	67.98	63.58	71.05	34.90	29.80	60.85	50.64	38.00	64.53	46.52	32.00	57.91	58.83	56.58
CLIP+ConvNext	54.45	1,511.08	63.83	67.41	63.63	70.80	35.09	30.40	59.91	51.32	35.00	64.45	47.88	33.33	57.25	56.32	59.08
SigLIP+DINOv2+ConvNext	53.78	1,450.64	63.57	67.79	63.63	71.34	34.80	30.20	61.04	49.32	37.70	64.05	45.83	30.00	56.21	58.08	54.33
SigLIP+CLIP+ConvNext	54.53	1,507.28	63.23	68.64	63.63	71.10	35.89	30.90	59.97	52.36	38.50	65.40	47.92	28.67	57.25	57.66	55.92

Table 3 | **All Benchmark Results for Model Ensemble with 1.2M Adapter Data + 737K Instruction Tuning Data.** Here, "SigLIP" = ViT-SO400M/14@384, "DINOv2" = ViT-L/14@518, "ConvNext" = OpenCLIP ConvNeXt-XXL@1024, and "CLIP" = OpenAI CLIP ViT-L/14@336.

3.5. Combining Multiple Vision Encoders

As observed in Fig. 6, different vision encoders excel in different aspects of MLLM performance. In this study, we explore the potential of combining multiple vision encoders to leverage their distinctive representations, aiming to build a more capable MLLM.

Given that different vision encoders use varying architectures and image resolutions, we interpolate to a fixed number of visual tokens (576) in this subsection (see details in Appendix D.3). We then concatenate these tokens along the feature dimension, following a method similar to A-MoF proposed in [117]. The results are tabulated in Table 3, where we observe consistent performance improvements with the addition of more models.

Our study indicates that adding a non-language-supervised model (DINOv2) can improve benchmark performance, especially in vision-centric tasks. Notably, even OCR benchmarks benefit from incorporating DINOv2. This highlights the importance of self-supervised learning models in complementing language-supervised models to achieve robust multimodal understanding. Detailed results and configurations are available in Appendix D.3.

However, this naive strategy has two limitations: 1) it employs interpolation, which can lead to information loss, especially with vision encoders with high-resolution feature maps, and 2) it treats each model equally via simple concatenation. Therefore, we seek a more effective strategy that can more flexibly leverage model combinations with less information loss.

> ***Finding 7:*** Combining multiple vision encoders, including vision SSL models, enhances MLLM performance across various benchmarks, particularly in vision-centric tasks.

4. Spatial Vision Aggregator (SVA): A New Connector Design

To effectively aggregate features from multiple vision encoders and prevent the information loss introduced by interpolation, we use a set of learnable latent queries that interact with multiple vision features via cross-attention layers [31]. In particular, our approach incorporates two new vision-centric design principles:

1. We introduce spatial inductive bias by explicitly defining the aggregation space for each token in the query.
2. We aggregate vision features multiple times across the LLM layers, enabling the model to repeatedly access and integrate necessary visual information.

Our new formulation flexibly accommodates multiple vision encoders with varying feature resolutions, while preserving the spatial structure of visual data during the aggregation process and its integration with the LLM. The method is elaborated below.

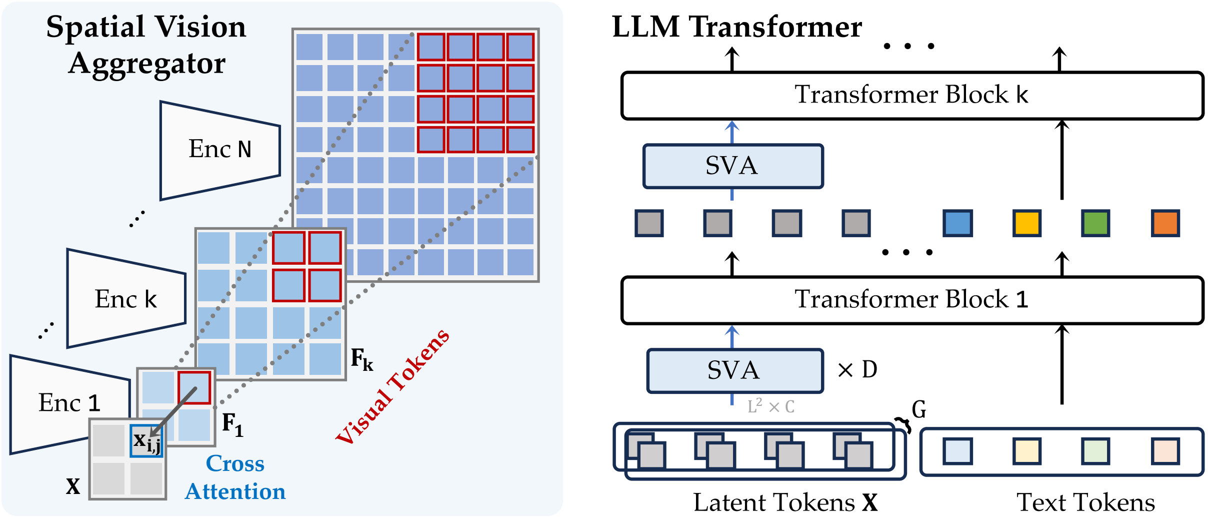

Figure 8 | **Spatial Vision Aggregator (SVA).** We propose SVA, a dynamic and spatially-aware connector that integrates multiple vision features with LLMs while reducing the number of tokens.

To facilitate information aggregation via cross-attention, we create a C-dimension learnable latent token $\mathbf{x} \in \mathbb{R}^{C}$ that is repeated $L \times L$ times to form a 2D grid, serving as the query $\mathbf{X} \in \mathbb{R}^{L^2 \times C}$. The set of visual features $\mathbf{F}$ from N vision encoders serve as the context (i.e., key and value). We ensure the output resolution of every vision encoder is a multiple of L. Formally, the feature map of the k-th vision encoder ($\mathbf{F}_k$) has a resolution of $m_k L \times m_k L \times C$, where m_k is a positive integer multiplier, and L is the height/width of the learnable 2D grid with hidden dimension C.

Spatial inductive bias To maintain the spatial structure during cross-attention, we align each token in the query with a specific sub-region of the feature maps in all vision encoders. Formally, a token at row i and column j in the query $\mathbf{x}_{i,j}$ corresponds to the sub-region

$$\mathbf{F}_k[m_k \cdot i : m_k \cdot (i+1), m_k \cdot j : m_k \cdot (j+1)] \in \mathbb{R}^{m_k^2 \times C}$$

of the k-th vision feature map. As a result, a token $\mathbf{x}_{i,j}$ aggregates a total of $\sum_k m_k^2$ features from N vision encoders through cross-attention (see Fig. 8-left).

Specifically, the updated query vector $\mathbf{q}^*_{\mathbf{i,j}} \in \mathbb{R}^{1 \times C}$ at position (i, j) is computed as

$$\mathbf{q}^*_{i,j} = \text{softmax}\left(\frac{\mathbf{q}_{i,j} \cdot \left[\mathbf{k}_{i,j,1}, \mathbf{k}_{i,j,2}, \dots, \mathbf{k}_{i,j,N}\right]^{\top}}{\sqrt{C}}\right)\left[\mathbf{v}_{i,j,1}, \mathbf{v}_{i,j,2}, \dots, \mathbf{v}_{i,j,N}\right], \tag{1}$$

where

$$\begin{aligned}
\mathbf{q}_{i,j} &= \mathbf{W}^{Q}\mathbf{x}_{\mathbf{i,j}} \in \mathbb{R}^{1 \times C},\\
\mathbf{k}_{i,j,k} &= \mathbf{W}^{K}_{k}\mathbf{F}_k[m_k \cdot i : m_k \cdot (i+1),\ m_k \cdot j : m_k \cdot (j+1)] \in \mathbb{R}^{m_k^2 \times C},\\
\mathbf{v}_{i,j,k} &= \mathbf{W}^{V}_{k}\mathbf{F}_k[m_k \cdot i : m_k \cdot (i+1),\ m_k \cdot j : m_k \cdot (j+1)] \in \mathbb{R}^{m_k^2 \times C}.
\end{aligned}$$

Here, $\mathbf{q}_{i,j}$ is the query vector at position (i, j), calculated using the query projection matrix $\mathbf{W}^{Q} \in \mathbb{R}^{C \times C}$. The key vectors $\mathbf{k}_{i,j,k}$ and value vectors $\mathbf{v}_{i,j,k}$ are computed for each vision encoder k using their respective key and value projection matrices $\mathbf{W}^{K}_{k} \in \mathbb{R}^{C \times C}$ and $\mathbf{W}^{V}_{k} \in \mathbb{R}^{C \times C}$. Since $\sum_k m_k^2$ features are aggregated into a single token, we effectively reduce the number of tokens.

Multi-layer vision aggregation Although our proposal effectively aggregates features from multiple vision encoders, there is still potential information loss with high-resolution input (large m_k) or multiple vision encoders (large N). Here, a single token would have to handle a larger amount of context information during aggregation. To prevent this, we allow cross-attention to occur multiple times by inserting our proposal throughout the LLM layers—allowing consistent access to the uncompressed visual information (see Fig. 8-right).

Hyperparameters To flexibly modulate capacity, we introduce two hyperparameters D and G, which indicate the number of cross-attention layers and distinct groups of learnable queries used between the vision models and the LLM, respectively. Intuitively, a larger D allows for more stacked cross-attention operations to facilitate the aggregation process, while a larger G enables a wider range of aggregation patterns to be captured. The G groups of queries aggregate visual information separately in parallel and then are concatenated to form the final visual tokens for the LLM. D and G are always set to 1 for cross-attention layers within LLM layers.

Connector	General	Knowledge	OCR & Chart	Vision-Centric
Concat. [117]	67.2	48.9	50.1	52.6
Resampler [51]	63.1	46.5	27.1	42.6
SVA-no-multi-agg	68.0	49.5	55.2	52.6
SVA	**68.5**	**49.7**	**55.5**	**53.2**

Table 4 | **Comparison between our SVA and other aggregation approaches.** The SVA module consistently outperforms other baselines and excels in aggregating high-resolution vision information.

We demonstrate the efficacy of SVA module using the best vision model combination results from the previous section and a Vicuna-1.5-7B base LLM. Specifically, we employ a combination of four vision encoders: OpenAI CLIP ViT-L/14@336, SigLIP ViT-SO400M/14@384, OpenCLIP ConvNeXt-XXL@1024, and DINOv2 ViT-L/14@518. We compare our method with two strong baselines: 1) concatenation-based [117] and 2) Re-sampler [10, 65], which utilizes a similar cross-attention form but lacks both spatial inductive biases and multi-layer vision aggregation. Here, we include two variants of our SVA module. The standard one, "**SVA**", uses $D = 3$, $G = 1$, and inserts cross-attention blocks inside the LLM with a layer stride of 3. To isolate the advantages of spatial inductive biases, we include another SVA variant, "SVA-no-multi-agg", that does not add cross-attention blocks inside the LLM and sets $D = 3$ and $G = 3$. Table 4 shows that SVA outperforms both baselines in all benchmark categories, with a significant improvement in the OCR & chart category (requiring high-resolution feature understanding). In contrast, the Resampler—which lacks spatial inductive biases—struggles to condense concatenated tokens from various vision towers into a limited number of learnable queries via global cross-attention.

D	OCR & Chart
2	52.1
3	52.4
4	**52.8**

(a) # layers

G	OCR & Chart
1	52.4
2	52.6
3	**53.1**

(b) # groups

Multi-agg	OCR & Chart
No	52.4
Yes	**53.3**

(c) Multi-layer aggregation

Table 5 | **Ablations on hyperparameter choices for SVA.** Enlarging the model capacity of the SVA module can further improve the performance.

We further conduct ablation experiments using OpenAI CLIP ViT-L/14@336 + OpenCLIP ConvNeXt-L@1024 as our base model combination. We focus on the OCR & chart categories to assess the impact on high-resolution visual understanding. The results show that increasing capacity via D or G improves performance and that allowing vision aggregation across multiple layers by adding cross-attention layers within the LLM also enhances performance. More detailed experimental setups and analyses are provided in the Appendix F.

Finding 8: Spatial inductive bias and deep interaction between LLM and vision feature help to better aggregate and condense vision features.

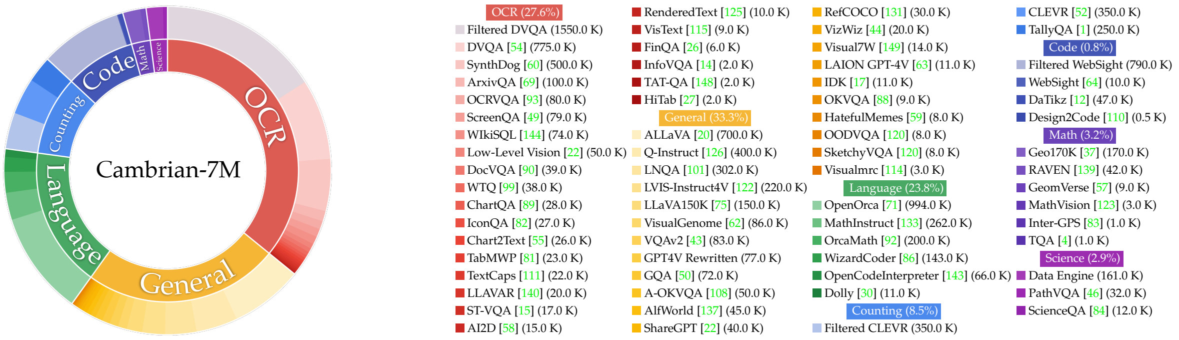

Figure 9 | **Cambrian-7M: A Large-Scale Curated Instruction Tuning Dataset for MLLM. Left:** The inner circle shows the original distribution of Cambrian-10M. The outer circle shows the curated Cambrian-7M. **Right:** All the data sources in the Cambrian dataset as well as the ones filtered in data curation.

5. Instruction Tuning Data for Training MLLMs

Previous work highlights the importance of data in training MLLMs [38, 73, 91], but explicit investigations are limited. Here, we gather all available instruction tuning data and examine data curation by enhancing diversity, balancing sources, and improving mixtures. Unless specified otherwise, experiments involve fine-tuning an OpenAI CLIP ViT-L/14@336px vision encoder [102] with a Vicuna-1.5-7B LLM base [142].

5.1. Data Collection

Collecting Instruction Tuning Data from existing data sources Unlike language data, multimodal (visual) instruction-tuning data is much rarer and harder to collect. To address this, we use existing multimodal benchmarks and datasets involving visual interaction data, such as Visual Question Answering (VQA) and OCR data. Previous work [138] highlights the catastrophic forgetting that commonly occurs when fine-tuning multimodal LLMs. To help maintain conversational abilities, we also collect a small volume of high-quality language-only instruction-following data. We categorize data into General conversation, OCR, Counting, Code, Math, Science, and Language-only data. We list the data sources in Fig. 9, and the details of data preparation in Appendix E.

Targeted Internet Data Collection Engine As observed in Fig. 9, there is an unbalanced distribution of data. Some categories, such as science, have very few data sources, and each source has limited samples. In the existing data sources, there are 32k samples in PathVQA [46] and 12k in ScienceQA [84]. This scarcity may be due to the difficulty of producing large-scale yet reliable scientific visual instruction tuning data. Previous work [66] has demonstrated the potential of using the internet to automatically gather targeted visual data for specific task; we employ similar ideas to address the scarcity, introducing a data engine to create large-scale, reliable, high-quality knowledge-based instruction tuning data (see Fig. 17). The engine selects a target field and subfield, such as "Physics", and uses an LLM like GPT-4 [95] to identify topics (e.g., "Newton's Laws"). It then searches reliable sources like Wikipedia for each topic. We find that image-text pairs extracted from Wikipedia pages are of high-quality. A parser extracts image-caption tuples and feeds the caption text to an LLM, such as GPT-3.5 [94], to generate instruction-type Q&A pairs about the image using an engineered prompt. These Q&A pairs and the image form our VQA dataset. Details are in Appendix E.3. Our data engine produces a large volume of reliable scientific data, increasing the diversity in the data pool. We generate 161k science-related data points—400% more than the previous combined data sources.

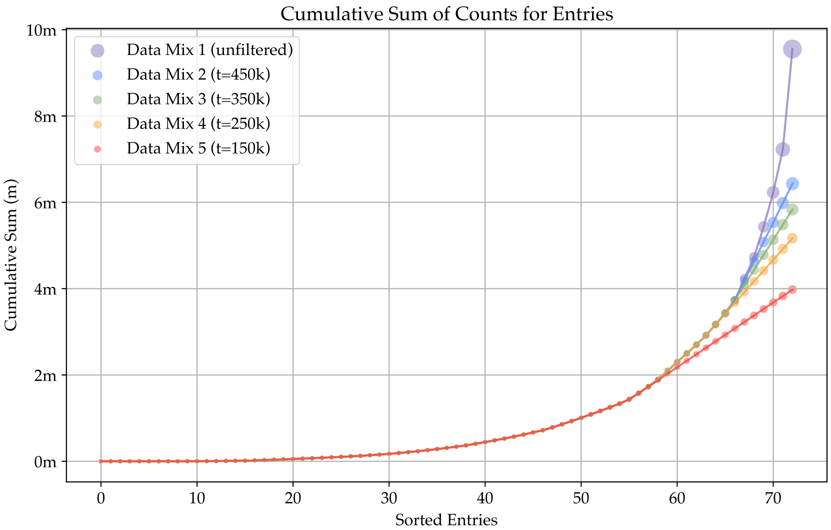

Figure 10 | **Data Balancing via Applying Thresholds on Data Sources**. Applying threshold t alleviates the exponential tail of Cambrian-10M.

	Average	General	Knowledge	OCR & Chart	Vision-Centric
150k	53.7	68.0	51.3	45.2	50.5
250k	**54.3**	**68.1**	51.5	45.3	52.2
350k	54.3	67.4	51.4	**46.0**	**52.3**
450k	54.2	68.0	**52.2**	45.5	50.7

Table 6 | **Threshold t value between 250k and 350k obtains better performance.** We observe an "elbow" effect in the data balancing experiment. A threshold t between 250k and 350k works best.

Cambrian-10M We create a large pool of instruction tuning data, which we refer to as Cambrian-10M. This pool contains approximately 9784k data points, offering a diverse range of data for our work and future research. We visualize its composition in Fig. 9.

5.2. Data Curation

Cambrian-10M is a large pool of instruction tuning data sourced from a variety of data sources, with an unbalanced data ratio between categories. Here, we take a preliminary step to study data curation by improving data balancing and adjusting data ratios.

Data Balancing We follow previous work [102, 129] to set thresholds t for the number of data points from a single data source. To study the effect of the number t, we plot the cumulative sum of counts for entries sorted by counts from tail to head (see Fig. 10). We choose t = 150k, 250k, 350k, and 450k in this section and observe an elbow effect in Table 6—finding that a threshold between 250k and 350k work the best for Cambrian-10M.

Data Ratio Unlike previous work in VLM data curation [36, 129] which curate noisy raw image-text pairs by scraping the internet, Cambrian-10M is designed for visual instruction tuning. Given the various capabilities of different types of data, it is essential to balance the ratio of these data types. We conduct pilot experiments with a fixed dataset size of 1350k, examining the impact of different data ratios on downstream performance. We visualize the results in Fig. 11 and summarize our findings as follows: (i) Balancing General, OCR and Language data is crucial. The model's OCR capability is proportional to the OCR data ratio; however, an excessive OCR ratio compromises general VQA and vision-centric performance. (ii) Performance on knowledge-intensive tasks is influenced by multiple factors, often requiring a mix of OCR, chart, reasoning, and general perception. Increasing the science data ratio can help, but a very low ratio leads to poor performance.

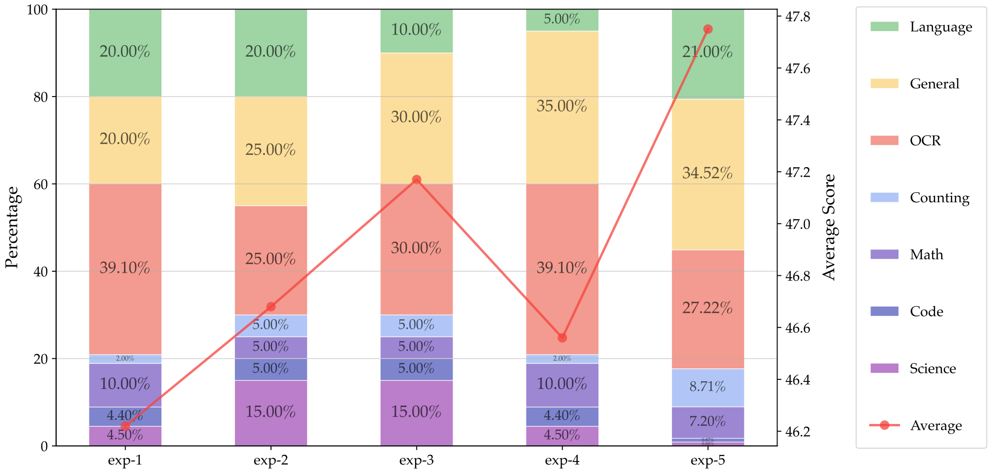

Figure 11 | **Exploring instruction tuning data mixture ratios.** We explore the impact of different ratios on the overall performance of the model with a controlled data size of 1.35M. We find that different ratios have a non-trivial impact on the overall performance, and exp-5 is the most optimal.

	Average	General	Knowledge	OCR & Chart	Vision-Centric
LLaVA-665K	40.7	64.7	45.2	20.8	32.0
Cambrian-10M	54.8	68.7	51.6	**47.3**	51.4
Cambrian-7M	**55.9**	**69.6**	**52.6**	**47.3**	**54.1**

Table 7 | **Performance improves with better instruction tuning data curation.** The model gains significant improvements when scaling up to Cambrian-10M. With data curation, the model further improves performance across all categories while enjoying more efficient training.

Cambrian-7M By applying data filtering to Cambrian-10M with our identified data ratio, we create a smaller but higher-quality dataset called Cambrian-7M. Table 7 showcases the benefits of a well-balanced and carefully curated dataset. Despite having fewer samples, Cambrian-7M demonstrates improved performance.

5.3. Alleviating the “Answer Machine Phenomenon” via System Prompts

Here, we investigate a phenomenon we term the “answer machine phenomenon”. We observe that a well-trained MLLM may excel at VQA benchmarks, but lack basic conversational abilities and default to outputting short, curt responses (see examples in Fig. 12). This discrepancy arises because benchmark questions typically require responses that are limited to a single option, choice, or word—diverging from the more broad and realistic use cases of MLLMs. Similar phenomena have been discussed in other LLM studies [106, 142, 146].

We suspect that this issue stems from instruction tuning data containing an excessive number of short-response VQA tasks, leading to catastrophic forgetting in LLMs. To address this, we incorporate additional system prompts during training. We append prompts such as “*Answer the question using a single word or phrase.*” before questions that generate a single word or phrase in the response. Full details of the system prompts used are provided in Appendix E.2. After integrating these system prompts, we observe that while the model’s benchmark performance remains unchanged, its conversational ability improves dramatically. For example, in Fig. 12, models with system prompts produce longer and more engaging responses while answering questions correctly. The system prompts also enhance the model’s performance on reasoning-related tasks, such as math problems, by encouraging a chain of thoughts [124] followed by the answer.

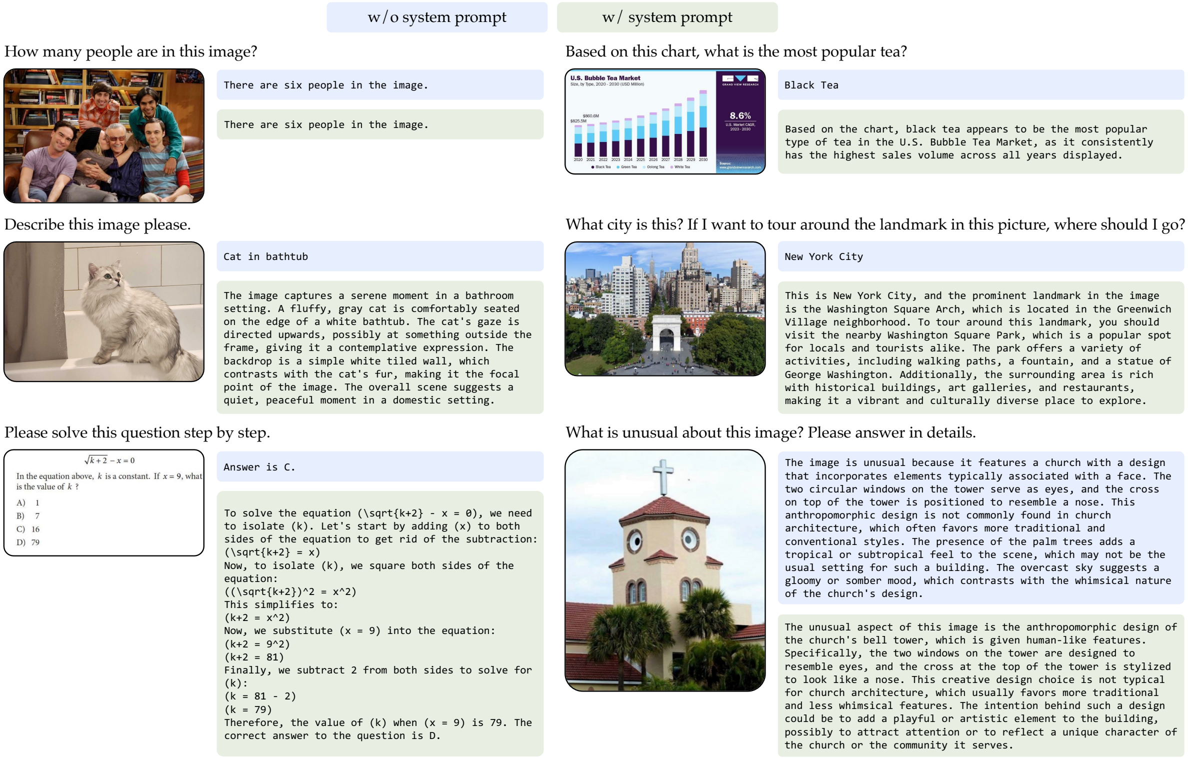

How many people are in this image?

```
There are six people in the image.
```

```
There are six people in the image.
```

Describe this image please.

```
Cat in bathtub
```

```
The image captures a serene moment in a bathroom
setting. A fluffy, gray cat is comfortably seated
on the edge of a white bathtub. The cat's gaze is
directed upwards, possibly at something outside the
frame, giving it a contemplative expression. The
backdrop is a simple white tiled wall, which
contrasts with the cat's fur, making it the focal
point of the image. The overall scene suggests a
quiet, peaceful moment in a domestic setting.
```

Please solve this question step by step.

$$\sqrt{k+2} - x = 0$$

In the equation above, k is a constant. If $x = 9$, what is the value of k ?

A) 1
B) 7
C) 16
D) 79

```
Answer is C.
```

```
To solve the equation (\sqrt{k+2} - x = 0), we need
to isolate (k). Let's start by adding (x) to both
sides of the equation to get rid of the subtraction:
(\sqrt{k+2} = x)
Now, to isolate (k), we square both sides of the
equation:
((\sqrt{k+2})^2 = x^2)
This simplifies to:
(k+2 = x^2)
Now, we substitute (x = 9) into the equation:
(k+2 = 9^2)
(k+2 = 81)
Finally, we subtract 2 from both sides to solve for
(k):
(k = 81 - 2)
(k = 79)
Therefore, the value of (k) when (x = 9) is 79. The
correct answer to the question is D.
```

Based on this chart, what is the most popular tea?

```
Black Tea
```

```
Based on the chart, black tea appears to be the most popular
type of tea in the U.S. Bubble Tea Market, as it consistently
has the highest sales volume across all years displayed.
```

What city is this? If I want to tour around the landmark in this picture, where should I go?

```
New York City
```

```
This is New York City, and the prominent landmark in the image
is the Washington Square Arch, which is located in the Greenwich
Village neighborhood. To tour around this landmark, you should
visit the nearby Washington Square Park, which is a popular spot
for locals and tourists alike. The park offers a variety of
activities, including walking paths, a fountain, and a statue of
George Washington. Additionally, the surrounding area is rich
with historical buildings, art galleries, and restaurants,
making it a vibrant and culturally diverse place to explore.
```

What is unusual about this image? Please answer in details.

```
The image is unusual because it features a church with a design
that incorporates elements typically associated with a face. The
two circular windows on the tower serve as eyes, and the cross
on top of the tower is positioned to resemble a nose. This
anthropomorphic design is not commonly found in church
architecture, which often favors more traditional and
conventional styles. The presence of the palm trees adds a
tropical or subtropical feel to the scene, which may not be the
usual setting for such a building. The overcast sky suggests a
gloomy or somber mood, which contrasts with the whimsical nature
of the church's design.
```

```
The unusual aspect of this image is the anthropomorphic design of
the church's bell tower, which is given human-like features.
Specifically, the two windows on the tower are designed to
resemble eyes, and the cross at the top of the tower is stylized
to look like a nose. This creative design choice is not typical
for church architecture, which usually favors more traditional
and less whimsical features. The intention behind such a design
could be to add a playful or artistic element to the building,
possibly to attract attention or to reflect a unique character of
the church or the community it serves.
```

Figure 12 | **Incorporating System Prompt in Instruction Tuning Data alleviates the "Answer Machine Phenomenon"** By adding system prompts in Cambrian-7M, the model exhibits better chat ability while retaining strong question answering abilities. The model without system prompts requires additional prompting to elicit longer responses.

This underscores the necessity of developing evaluation protocols like the Chatbot Arena [29] for MLLMs, despite the challenges in collecting large-scale, real-world interaction data. While performing well on benchmarks is important, it is equally crucial to ensure the model can engage in meaningful and natural interactions. The overall user experience and the model's conversational abilities are paramount, as a model that excels in benchmarks but fails to converse effectively cannot meet the needs of practical applications.

6. State of the Art Performance

Finally, we leverage the insights from all our previous studies to train a family of MLLMs we call Cambrian-1. We train models using LLM backbones of various scales: LLaMA-3-Instruct-8B [3], Vicuna-1.5-13B [142], and Hermes-2-Yi-34B [130]. Our vision component combines four models—OpenAI CLIP ViT-L/14@336, SigLIP ViT-SO400M/14@384, OpenCLIP ConvNeXt-XXL@1024, and DINOv2 ViT-L/14@518 (Section 3.5)—via the Spatial Vision Aggregator (Section 4). We pre-train the connector using 2.5M adapter data and instruction tune using our Cambrian-7M data mix (Section 5.2). Our models are evaluated on the benchmarks categorized in Section 3.1, with results presented in Table 8 and Fig. 13[6].

Cambrian-1 surpasses open-source models like LLaVA-NeXT and Mini-Gemini. Thanks to the SVA, Cambrian-1 excels in tasks requiring high-resolution image processing, even with only 576 image tokens—about 1/5 of the tokens used by LLaVA-NeXT and Mini-Gemini. Cambrian-1 also achieves comparable performance to the best proprietary models, such as GPT-4V, Gemini-

[6] For the General Average, we note that GPT-4's performance on the GQA test set is low, possibly because other models are trained on the GQA training set, whereas the training set used for GPT-4 is unclear.

Model		General					Knowledge					OCR & Chart					Vision-Centric				
Method	# Vis Tok.	Avg	MME^{P}	MMB	SEED^{I}	GQA	Avg	SQA^{I}	MMMU^{V}	$\text{MathVista}^{\text{M}}$	AI2D	Avg	ChartQA	OCRBench	TextVQA	DocVQA	Avg	MMVP	RealworldQA	$\text{CV-Bench}^{\text{2D}}$	$\text{CV-Bench}^{\text{3D}}$
GPT-4V	UNK.	63.0	1409.4	75.8	69.1	36.8	65.2	75.7	56.8	49.9	78.2	77.4	78.5	64.5	78.0	88.4	62.4	50.0	61.4	64.3	73.8
Gemini-1.0 Pro	UNK.	-	1496.6	73.6	70.7	-	-	79.5	47.9	45.2	-	-	-	65.9	-	-	-	-	-	-	-
Gemini-1.5 Pro	UNK.	-	-	-	-	-	-	-	58.5	52.1	80.3	-	81.3	-	73.5	86.5	-	-	67.5	-	-
Grok-1.5	UNK.	-	-	-	-	-	-	-	53.6	52.8	88.3	-	76.1	-	78.1	85.6	-	-	68.7	-	-
MM-1-8B	144	-	1529.3	72.3	69.9	-	-	72.6	37.0	35.9	-	-	-	-	-	-	-	-	-	-	-
MM-1-30B	144	-	1637.6	75.1	72.1	-	-	81.0	44.7	39.4	-	-	-	-	-	-	-	-	-	-	-
Base LLM: Llama-3-Ins-8B																					
Mini-Gemini-HD-8B	2880	72.7	**1606.0**	72.7	73.2	64.5	55.7	75.1	37.3	37.0	**73.5**	62.9	59.1	47.7	70.2	74.6	51.5	18.7	62.1	62.2	63.0
LLaVA-NeXT-8B	2880	72.5	1603.7	72.1	72.7	**65.2**	55.6	72.8	41.7	36.3	71.6	63.9	69.5	49.0	64.6	72.6	56.6	38.7	60.1	62.2	65.3
Cambrian-1-8B	576	**73.1**	1,547.1	**75.9**	**74.7**	64.6	**61.3**	**80.4**	**42.7**	**49.0**	73.0	**71.3**	**73.3**	**62.4**	**71.7**	**77.8**	**65.0**	**51.3**	**64.2**	**72.3**	**72.0**
Base LLM: Vicuna-1.5-13B																					
Mini-Gemini-HD-13B	2880	70.7	1597.0	68.6	70.6	63.7	54.1	71.9	37.3	37.0	70.1	60.8	56.6	46.6	70.2	69.8	49.4	19.3	57.5	53.6	67.3
LLaVA-NeXT-13B	2880	69.9	1575.0	70.0	65.6	**65.4**	53.7	73.5	36.2	35.1	70.0	62.9	62.2	51.4	67.1	70.9	55.9	36.0	59.1	62.7	65.7
Cambrian-1-13B	576	**73.7**	**1,610.4**	**75.7**	**74.4**	64.3	**60.2**	**79.3**	**40.0**	**48.0**	**73.6**	**71.3**	**73.8**	**61.9**	**72.8**	**76.8**	**62.2**	**41.3**	**63.0**	**72.5**	**71.8**
Base LLM: Hermes2-Yi-34B																					
Mini-Gemini-HD-34B	2880	76.2	1659.0	80.6	75.3	65.8	62.4	77.7	48.0	43.4	**80.5**	68.1	67.6	51.8	74.1	**78.9**	63.8	37.3	67.2	71.5	79.2
LLaVA-NeXT-34B	2880	76.0	1633.2	79.3	**75.9**	**67.1**	62.5	81.8	46.7	46.5	74.9	67.7	68.7	54.5	69.5	78.1	64.0	47.3	61.0	73.0	74.8
Cambrian-1-34B	576	**76.8**	**1689.3**	**81.4**	75.3	65.8	**67.0**	**85.6**	**49.7**	**53.2**	79.7	**71.9**	**75.6**	**60.0**	**76.7**	75.5	**68.5**	**52.7**	**67.8**	**74.0**	**79.7**

Table 8 | **Comparison of Cambrian-1 with other leading MLLM framework.** Cambrian-1 outperforms other open-source models and achieves competitive performance on a number of benchmarks, compared to proprietary models such as GPT-4V, Gemini, and Grok-1.5. Despite using only 576 visual tokens, Cambrian-1 performs better on OCR & Chart and Vision-Centric benchmarks compared to Mini-Gemini-HD and LLaVA-NeXT, which use 2880 tokens.

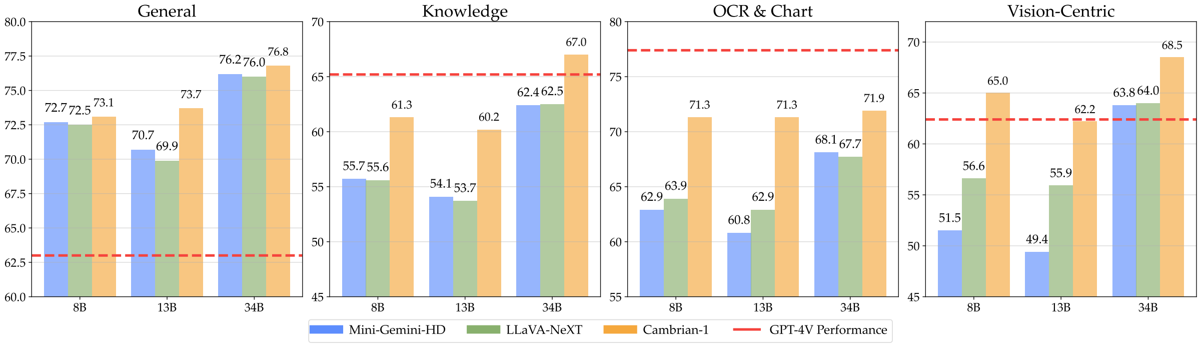

Figure 13 | **Comparison of model average performances on each category.** Cambrian-1 outperforms other open-source models across all sizes. The lead is especially large on OCR & Chart and Vision-Centric benchmarks, highlighting the advantage of our vision-centric design.

Pro, and MM-1, on several benchmarks. We showcase some examples in Fig. 14, demonstrating that the model effectively attends to details in images despite using only 576 tokens.

Additionally, we emphasize the importance of post-processing a model's output and assessing its accuracy. For instance, if the correct answer is `"(a) Apple"` and the model outputs `"Apple"`, it is crucial to recognize the response as correct. We use fuzzy matching to evaluate the accuracy of our model's outputs and conduct an ablation study with LLMs like GPT-3.5 to validate this method. Our findings indicate that fuzzy matching provides reliable judgments. Further details can be found in Appendix G.2.

7. Discussion

We advocate for using MLLMs as an interface to evaluate visual representations, as previous benchmarks are becoming saturated and do not adequately reflect the diverse and complex perception challenges of the real world. Our work highlights the current gap between language-supervised models and self-supervised learning models and demonstrates the potential of

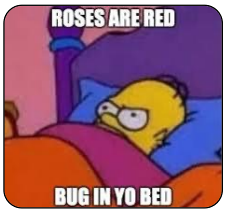

Why is this image funny?

```
The humor in this image comes from the
unexpected twist on the classic poem
'Roses are red, violets are blue.' Instead
of a romantic or sweet sentiment, the poem
is humorously altered to a more mundane
and slightly unsettling scenario, which is
a bug in the bed. This juxtaposition of a
traditional romantic poem with a common,
albeit slightly unpleasant, household
occurrence creates a comedic effect.
```

Which character is this?

```
The character in the image is Homer Simpson,
a central character from the animated
television series 'The Simpsons.' Homer is
known for his distinctive yellow skin,
casual attire, and often humorous or
oblivious behavior.
```

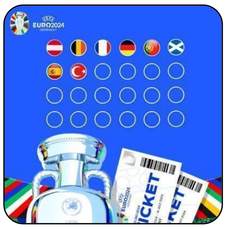

List all the countries in this image in the format of a json {1: 2:, etc}. Why are the flags here?

```
{
"1": "Austria",
"2": "Belgium",
"3": "France",
"4": "Germany",
"5": "Portugal",
"6": "Scotland",
"7": "Spain",
"8": "Turkey"
}
The flags are here to represent the
participating countries in the UEFA EURO
2024 tournament, which is hosted by
Germany. Each flag corresponds to a
country that is either a host or a
participant in the event, as indicated by
the tickets below the flags. The tickets
suggest that these countries are either
hosting matches or have qualified to play
in the tournament.
```

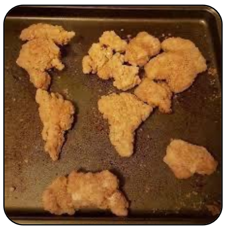

What does this image remind you of?

```
The image might remind you of a playful
and creative culinary presentation,
possibly inspired by a world map, where
each piece of food represents a different
continent. It could also evoke thoughts of
a fun cooking challenge or a themed meal
where the food is arranged to mimic the
shape of the Earth.
```

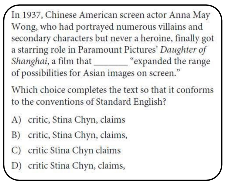

In 1937, Chinese American screen actor Anna May Wong, who had portrayed numerous villains and secondary characters but never a heroine, finally got a starring role in Paramount Pictures' *Daughter of Shanghai*, a film that ______ "expanded the range of possibilities for Asian images on screen."

Which choice completes the text so that it conforms to the conventions of Standard English?

A) critic, Stina Chyn, claims
B) critic, Stina Chyn, claims,
C) critic Stina Chyn claims
D) critic Stina Chyn, claims,

Please solve the problem step by step:

```
To solve this problem, we need to
determine which option correctly completes
the sentence in a way that adheres to the
conventions of Standard English. The
sentence is:
"In 1937, Chinese American screen actor
Anna May Wong, who had portrayed numerous
villains and secondary characters but
never a heroine, finally got a starring
role in Paramount Pictures' Daughter of
Shanghai, a film that _____ "expanded the
range of possibilities for Asian images on
screen."
The correct option should be the one that
maintains the subject-verb agreement and
the appropriate punctuation.
Option A: "critic, Stina Chyn, claims" -
This option is incorrect because it uses a
comma after the name, which is not
standard in English.
Option B: "critic, Stina Chyn, claims," -
This option is also incorrect because it
uses a comma after the name and an extra
comma at the end of the sentence, which is
not standard in English.
Option C: "critic Stina Chyn claims" -
This option is correct because it
maintains the subject-verb agreement and
does not use any unnecessary commas.
Option D: "critic Stina Chyn, claims," -
This option is incorrect because it uses a
comma after the name and an extra comma at
the end of the sentence, which is not
standard in English.
Therefore, the correct answer is Option C:
"critic Stina Chyn claims."
```

Figure 14 | **Examples of Cambrian-1-34B.** Cambrian-1 showcases impressive abilities in visual intersection. The model demonstrates instruction-following ability such as output in json format, as illustrated in the bottom-left example. Cambrian-1 also demonstrates remarkable OCR ability (See model handles different Comma "," in the right down example).

bridging this gap. However, it is known that features of language-supervised models behave like a *bag-of-words* [116, 135], underscoring the need for advancements in vision-only models to ensure better visual understanding. We hope to inspire future research into developing better vision-only models intended to be adapted into the MLLM setting, that more effectively leverage large-scale datasets [78] and preserve the advantages in visual grounding [117].

As we observe in Table 8, a well-trained open-source model such as Cambrian-1 can match or even outperform proprietary models on many existing benchmarks. However, the use and evaluation of MLLMs extend far beyond the current scope of benchmarks—to conversational ability, creativity, reliability, and overall user experience. Developing models solely based on benchmark results can result in an "answer machine", over-optimized for benchmarks but lacking in practical interaction capabilities. Therefore, the development of MLLMs that better align with human and societal needs is a continuously evolving process, both in terms of evaluation and model development.

Our current Cambrian-1 model uses a moderate number of visual tokens and does not adopt the any-resolution strategy [25, 70, 74] to handle ultra high-resolution images or those with extreme aspect ratios, which require a larger number of visual tokens. For specialized tasks like V*Bench [127], which require processing ultra high-resolution images, increasing the resolution and number of visual tokens could lead to an HD version of the Cambrian-1 model.

One promising direction for post-training alignment is through reinforcement learning rather than supervised fine-tuning. Many MLLM studies, including Cambrian, primarily focus on supervised fine-tuning. Yet, recent advancements in LLMs [32, 97, 103, 147] and some in MLLMs [132, 137] suggest that reinforcement learning from human or environmental feedback can further improve models, potentially surpassing the limits of supervised fine-tuning, especially in decision-making abilities.

Cambrian-10M (Fig. 9 and Section 5) provides a rich pool of data for studying data curation in fine-tuning MLLMs. Our work takes an initial step in curating higher-quality data to enable more efficient and effective instruction tuning. We believe there is room for further improvement in the data curation pipeline, and we hope this work can serve as a foundation for future research.

Additionally, training large-scale models requires careful design of model sharding, data sharding, and infrastructure adaptations. In this work, we train our model on TPU-V4 [53] with FSDP [141] using TorchXLA. We share our experiences, technical challenges, and solutions in Appendix A. We also open-source our implementation and provide tutorials to help the community undertake large-scale training more efficiently.

To conclude, Cambrian-1 introduces a family of state-of-the-art MLLM models that achieve top performance across diverse benchmarks and excel in visual-centric tasks. We provide model weights, open-source code, datasets, and detailed recipes for model training and evaluation. We hope our work will strengthen the open research community and accelerate future advancements in both visual representation learning and multimodal systems.

Acknowledgements

We are grateful to LLaVA [75] for their excellent codebase, which served as the launching point for our research. Special thanks to Hexu Zhao for extensive discussions and knowledge-sharing around FSDP and large-scale training techniques, and to Jiasen Lu for helpful discussions on TPU and JAX distributed training infrastructure. We also appreciate the assistance and responses from the PyTorchXLA team via GitHub.

We are thankful to Kaiming He for early discussions on multi-modal large language models. We also thank Zhuang Liu, Junlin Han, Yuexiang Zhai, Tianzhe Chu, Daohan Lu, Weiyang Jin, Boyang Zhang, and Jiayi Pan for reviewing this manuscript. We also acknowledge DeepSeek [80] for the paper template inspiration.

This work was primarily supported by the Google TPU Research Cloud (TRC) program and the Google Cloud Research Credits program (GCP19980904). Additional support was provided by the NYU IT High Performance Computing resources, services, and staff expertise. S.X. would like to thank the OpenAI Researcher Access program, Open Path AI Foundation, and an Amazon Research award for their support. S.T. is supported by the OpenAI SuperAlignment Fellowship, and E.B. is supported by the NDSEG Fellowship.

References

[1] M. Acharya, K. Kafle, and C. Kanan. “TallyQA: Answering complex counting questions”. In: *AAAI*. 2019.

[2] A. Agrawal et al. “Don’t just assume; look and answer: Overcoming priors for visual question answering”. In: *CVPR*. 2018.

[3] AI@Meta. “Llama 3 Model Card”. In: (2024).

[4] H. A. Alawwad et al. “Enhancing Textbook Question Answering Task with Large Language Models and Retrieval Augmented Generation”. In: *arXiv preprint arXiv:2402.05128* (2024).

[5] J.-B. Alayrac et al. “Flamingo: a visual language model for few-shot learning”. In: *NeurIPS*. 2022.

[6] T. Aquinas. *Quaestiones Disputatae de Veritate*. q.2 a.3 arg.19, 1259.

[7] Aristotle. *Metaphysics*. Ed. by T. by W. D. Ross. The Internet Classics Archive, 350BCE.

[8] M. Assran et al. “Self-supervised learning from images with a joint-embedding predictive architecture”. In: *CVPR*. 2023.

[9] J. Bai et al. “Qwen Technical Report”. In: *arXiv preprint arXiv:2309.16609* (2023).

[10] J. Bai et al. “Qwen-vl: A versatile vision-language model for understanding, localization, text reading, and beyond”. In: (2023).

[11] M. E. Banani et al. “Probing the 3D Awareness of Visual Foundation Models”. In: *arXiv preprint arXiv:2404.08636* (2024).

[12] J. Belouadi, A. Lauscher, and S. Eger. “Automatikz: Text-guided synthesis of scientific vector graphics with tikz”. In: *ICLR*. 2024.

[13] R. Birkl, D. Wofk, and M. Müller. “Midas v3. 1–a model zoo for robust monocular relative depth estimation”. In: *arXiv preprint arXiv:2307.14460* (2023).

[14] A. F. Biten et al. “Latr: Layout-aware transformer for scene-text vqa”. In: *CVPR*. 2022.

[15] A. F. Biten et al. “Scene text visual question answering”. In: *ICCV*. 2019.

[16] G. Brazil et al. “Omni3d: A large benchmark and model for 3d object detection in the wild”. In: *CVPR*. 2023.

[17] S. Cha et al. “Visually Dehallucinative Instruction Generation: Know What You Don’t Know”. In: *arXiv preprint arXiv:2402.09717* (2024).

[18] D. J. Chalmers. “Does Thought Require Sensory Grounding? From Pure Thinkers to Large Language Models”. In: *Proceedings and Addresses of the American Philosophical Association* 97 (2023), pp. 22–45.

[19] Y. Chang et al. “A survey on evaluation of large language models”. In: *ACM Transactions on Intelligent Systems and Technology* 15.3 (2024), pp. 1–45.

[20] G. H. Chen et al. “ALLaVA: Harnessing GPT4V-synthesized Data for A Lite Vision-Language Model”. In: *arXiv preprint arXiv:2402.11684* (2024).

[21] L. Chen et al. “Are We on the Right Way for Evaluating Large Vision-Language Models?” In: *arXiv preprint arXiv:2403.20330* (2024).

[22] L. Chen et al. “Sharegpt4v: Improving large multi-modal models with better captions”. In: *arXiv preprint arXiv:2311.12793* (2023).

[23] X. Chen et al. “Pali: A jointly-scaled multilingual language-image model”. In: *ICLR*. 2023.

[24] X. Chen, S. Xie, and K. He. “An empirical study of training self-supervised vision transformers”. In: *ICCV*. 2021.

[25] Z. Chen et al. "How far are we to gpt-4v? closing the gap to commercial multimodal models with open-source suites". In: *arXiv preprint arXiv:2404.16821* (2024).

[26] Z. Chen et al. "Finqa: A dataset of numerical reasoning over financial data". In: *EMNLP*. 2021.

[27] Z. Cheng et al. "HiTab: A hierarchical table dataset for question answering and natural language generation". In: *ACL*. 2022.

[28] M. Cherti et al. "Reproducible scaling laws for contrastive language-image learning". In: *CVPR*. 2023.

[29] W.-L. Chiang et al. "Chatbot arena: An open platform for evaluating llms by human preference". In: *arXiv preprint arXiv:2403.04132* (2024).

[30] M. Conover et al. *Free Dolly: Introducing the World's First Truly Open Instruction-Tuned LLM*. 2023. URL: https://www.databricks.com/blog/2023/04/12/dolly-first-open-commercially-viable-instruction-tuned-llm (visited on 06/30/2023).

[31] W. Dai et al. "Instructblip: Towards general-purpose vision-language models with instruction tuning". In: *NeurIPS*. 2024.

[32] H. Dong et al. "Rlhf workflow: From reward modeling to online rlhf". In: *arXiv preprint arXiv:2405.07863* (2024).

[33] A. Dosovitskiy et al. "An image is worth 16x16 words: Transformers for image recognition at scale". In: *ICLR*. 2021.

[34] A. Fang et al. "Data filtering networks". In: *ICLR*. 2024.

[35] X. Fu et al. "BLINK: Multimodal Large Language Models Can See but Not Perceive". In: *arXiv preprint arXiv:2404.12390* (2024).

[36] S. Y. Gadre et al. "Datacomp: In search of the next generation of multimodal datasets". In: vol. 36. 2024.

[37] J. Gao et al. "G-llava: Solving geometric problem with multi-modal large language model". In: *arXiv preprint arXiv:2312.11370* (2023).

[38] P. Gao et al. "SPHINX-X: Scaling Data and Parameters for a Family of Multi-modal Large Language Models". In: *arXiv preprint arXiv:2402.05935* (2024).

[39] Y. Ge et al. "Planting a seed of vision in large language model". In: *arXiv preprint arXiv:2307.08041* (2023).

[40] R. Geirhos et al. "Shortcut learning in deep neural networks". In: *Nature Machine Intelligence* (2020).

[41] R. Girshick et al. "Rich feature hierarchies for accurate object detection and semantic segmentation". In: *CVPR*. 2014.

[42] Google. *Gemini*. 2023.

[43] Y. Goyal et al. "Making the v in vqa matter: Elevating the role of image understanding in visual question answering". In: *CVPR*. 2017.

[44] D. Gurari et al. "Vizwiz grand challenge: Answering visual questions from blind people". In: *CVPR*. 2018.

[45] K. He et al. "Masked autoencoders are scalable vision learners". In: *CVPR*. 2022.

[46] X. He et al. "PathVQA: 30000+ Questions for Medical Visual Question Answering". In: *CoRR* abs/2003.10286 (2020).

[47] T. Hiippala et al. "AI2D-RST: A multimodal corpus of 1000 primary school science diagrams". In: *Language Resources and Evaluation* 55 (2021), pp. 661–688.

[48] J. Hoffmann et al. "Training compute-optimal large language models". In: *NeurIPS* (2023).

[49] Y.-C. Hsiao, F. Zubach, M. Wang, et al. "Screenqa: Large-scale question-answer pairs over mobile app screenshots". In: *arXiv preprint arXiv:2209.08199* (2022).

[50] D. A. Hudson and C. D. Manning. "GQA: A New Dataset for Real-World Visual Reasoning and Compositional Question Answering". In: *CVPR*. 2019.

[51] A. Jaegle et al. "Perceiver: General perception with iterative attention". In: *ICML*. 2021.

[52] J. Johnson et al. "Clevr: A diagnostic dataset for compositional language and elementary visual reasoning". In: *CVPR*. 2017.

[53] N. Jouppi et al. "Tpu v4: An optically reconfigurable supercomputer for machine learning with hardware support for embeddings". In: *Proceedings of the 50th Annual International Symposium on Computer Architecture*. 2023.

[54] K. Kafle et al. "Dvqa: Understanding data visualizations via question answering". In: *CVPR*. 2018.

[55] S. Kantharaj et al. "Chart-to-text: A large-scale benchmark for chart summarization". In: *ACL*. 2022.

[56] S. Karamcheti et al. "Prismatic vlms: Investigating the design space of visually-conditioned language models". In: *arXiv preprint arXiv:2402.07865* (2024).

[57] M. Kazemi et al. "Geomverse: A systematic evaluation of large models for geometric reasoning". In: 2023.

[58] A. Kembhavi et al. "A diagram is worth a dozen images". In: *ECCV*. 2016.

[59] D. Kiela et al. "The hateful memes challenge: Detecting hate speech in multimodal memes". In: *NeurIPS*. 2020.

[60] G. Kim et al. "Donut: Document understanding transformer without ocr". In: *ECCV*. 2022.

[61] A. Kirillov et al. "Segment anything". In: *ICCV*. 2023.

[62] R. Krishna et al. "Visual Genome: Connecting Language and Vision Using Crowdsourced Dense Image Annotations". In: *IJCV* (2016).

[63] LAION. *laion/gpt4v-dataset*. 2023.

[64] H. Laurençon, L. Tronchon, and V. Sanh. "Unlocking the conversion of Web Screenshots into HTML Code with the WebSight Dataset". In: *arXiv preprint arXiv:2403.09029* (2024).

[65] H. Laurençon et al. "What matters when building vision-language models?" In: *arXiv preprint arXiv:2405.02246* (2024).

[66] A. C. Li et al. "Internet Explorer: Targeted Representation Learning on the Open Web". In: *ICML*. 2023.

[67] A. C. Li et al. "Your diffusion model is secretly a zero-shot classifier". In: *ICCV*. 2023.

[68] B. Li et al. *LLaVA-NeXT: Stronger LLMs Supercharge Multimodal Capabilities in the Wild*. 2024.

[69] L. Li et al. "Multimodal ArXiv: A Dataset for Improving Scientific Comprehension of Large Vision-Language Models". In: *arXiv preprint arXiv:2403.00231* (2024).

[70] Y. Li et al. "Mini-gemini: Mining the potential of multi-modality vision language models". In: *arXiv preprint arXiv:2403.18814* (2024).

[71] W. Lian et al. *OpenOrca: An Open Dataset of GPT Augmented FLAN Reasoning Traces*. `https://https://huggingface.co/Open-Orca/OpenOrca`. 2023.

[72] T.-Y. Lin et al. “Microsoft coco: Common objects in context”. In: *ECCV*. 2014.

[73] H. Liu et al. “Improved baselines with visual instruction tuning”. In: *arXiv preprint arXiv:2310.03744* (2023).

[74] H. Liu et al. *LLaVA-NeXT: Improved reasoning, OCR, and world knowledge*. 2024.

[75] H. Liu et al. “Visual Instruction Tuning”. In: *NeurIPS*. 2023.

[76] Y. Liu et al. “Mmbench: Is your multi-modal model an all-around player?” In: *arXiv preprint arXiv:2307.06281* (2023).

[77] Y. Liu et al. “On the hidden mystery of ocr in large multimodal models”. In: *arXiv preprint arXiv:2305.07895* (2023).

[78] Z. Liu and K. He. “A Decade’s Battle on Dataset Bias: Are We There Yet?” In: *arXiv preprint arXiv:2403.08632* (2024).

[79] Z. Liu et al. “A convnet for the 2020s”. In: *CVPR*. 2022.

[80] H. Lu et al. “DeepSeek-VL: towards real-world vision-language understanding”. In: *arXiv preprint arXiv:2403.05525* (2024).

[81] P. Lu et al. “Dynamic prompt learning via policy gradient for semi-structured mathematical reasoning”. In: *ICLR*. 2023.

[82] P. Lu et al. “Iconqa: A new benchmark for abstract diagram understanding and visual language reasoning”. In: *NeurIPS*. 2021.

[83] P. Lu et al. “Inter-GPS: Interpretable geometry problem solving with formal language and symbolic reasoning”. In: *ACL*. 2021.

[84] P. Lu et al. “Learn to explain: Multimodal reasoning via thought chains for science question answering”. In: *NeurIPS*. 2022.

[85] P. Lu et al. “Mathvista: Evaluating mathematical reasoning of foundation models in visual contexts”. In: *ICLR* (2023).

[86] Z. Luo et al. “Wizardcoder: Empowering code large language models with evol-instruct”. In: *ICLR*. 2024.

[87] A. Majumdar et al. “OpenEQA: Embodied Question Answering in the Era of Foundation Models”. In: *2nd Workshop on Mobile Manipulation and Embodied Intelligence at ICRA 2024*. 2024.

[88] K. Marino et al. “OK-VQA: A Visual Question Answering Benchmark Requiring External Knowledge”. In: *CVPR*. 2019.

[89] A. Masry et al. “Chartqa: A benchmark for question answering about charts with visual and logical reasoning”. In: *ACL*. 2022.

[90] M. Mathew, D. Karatzas, and C. Jawahar. “Docvqa: A dataset for vqa on document images”. In: *WACV*. 2021.

[91] B. McKinzie et al. “Mm1: Methods, analysis & insights from multimodal llm pretraining”. In: *arXiv preprint arXiv:2403.09611* (2024).

[92] A. Mitra et al. *Orca-Math: Unlocking the potential of SLMs in Grade School Math*. 2024. arXiv: 2402.14830 [cs.CL].

[93] “OCR-VQA: Visual Question Answering by Reading Text in Images”. In: 2019.

[94] OpenAI. *ChatGPT*. 2022.

[95] OpenAI. *gpt4o*. 2024.

[96] M. Oquab et al. “Dinov2: Learning robust visual features without supervision”. In: *TMLR* (2023).

[97] L. Ouyang et al. “Training language models to follow instructions with human feedback”. In: *NeurIPS*. 2022.

[98] A. Parker. *In the blink of an eye: how vision sparked the big bang of evolution*. 2003.

[99] P. Pasupat and P. Liang. “Compositional semantic parsing on semi-structured tables”. In: *ACL*. 2015.

[100] J. Piaget, M. Cook, et al. *The origins of intelligence in children*. Vol. 8. 5. International Universities Press New York, 1952.

[101] J. Pont-Tuset et al. “Connecting Vision and Language with Localized Narratives”. In: *ECCV*. 2020.

[102] A. Radford et al. “Learning transferable visual models from natural language supervision”. In: *ICML*. 2021.

[103] R. Rafailov et al. “Direct preference optimization: Your language model is secretly a reward model”. In: *NeurIPS*. 2024.

[104] R. Rombach et al. “High-Resolution Image Synthesis With Latent Diffusion Models”. In: *CVPR*. 2022.

[105] O. Russakovsky et al. “Imagenet large scale visual recognition challenge”. In: *IJCV* (2015).

[106] O. Sanseviero. *LLM Evals and Benchmarking*. 2022.

[107] C. Schuhmann et al. “Laion-5b: An open large-scale dataset for training next generation image-text models”. In: *NeurIPS*. 2022.

[108] D. Schwenk et al. “A-OKVQA: A Benchmark for Visual Question Answering using World Knowledge”. In: *ECCV*. 2022.

[109] M. Shridhar et al. “ALFWorld: Aligning Text and Embodied Environments for Interactive Learning”. In: *ICLR*. 2021.

[110] C. Si et al. “Design2Code: How Far Are We From Automating Front-End Engineering?” In: *arXiv preprint arXiv:2403.03163* (2024).

[111] O. Sidorov et al. *TextCaps: a Dataset for Image Captioning with Reading Comprehension*. 2020. arXiv: `2003.12462 [cs.CV]`.

[112] A. Singh et al. “Towards vqa models that can read”. In: *CVPR*. 2019.

[113] Q. Sun et al. “Eva-clip: Improved training techniques for clip at scale”. In: *arXiv preprint arXiv:2303.15389* (2023).

[114] R. Tanaka, K. Nishida, and S. Yoshida. “VisualMRC: Machine Reading Comprehension on Document Images”. In: *AAAI*. 2021.

[115] B. J. Tang, A. Boggust, and A. Satyanarayan. “Vistext: A benchmark for semantically rich chart captioning”. In: *arXiv preprint arXiv:2307.05356* (2023).

[116] S. Tong, E. Jones, and J. Steinhardt. “Mass-producing failures of multimodal systems with language models”. In: *NeurIPS*. 2024.

[117] S. Tong et al. “Eyes wide shut? exploring the visual shortcomings of multimodal llms”. In: *CVPR*. 2024.

[118] H. Touvron et al. “LLaMA 2: Open foundation and fine-tuned chat models”. In: (2023).

[119] H. Touvron et al. “LLaMA: Open and efficient foundation language models”. In: *arXiv preprint arXiv:2302.13971* (2023).

[120] H. Tu et al. “How many unicorns are in this image? a safety evaluation benchmark for vision llms”. In: *arXiv preprint arXiv:2311.16101* (2023).

[121] K. Vishniakov, Z. Shen, and Z. Liu. “ConvNet vs Transformer, Supervised vs CLIP: Beyond ImageNet Accuracy”. In: *ICML*. 2024.

[122] J. Wang et al. “To see is to believe: Prompting gpt-4v for better visual instruction tuning”. In: *arXiv preprint arXiv:2311.07574* (2023).

[123] K. Wang et al. “Measuring Multimodal Mathematical Reasoning with MATH-Vision Dataset”. In: *arXiv preprint arXiv:2402.14804* (2024).

[124] J. Wei et al. “Chain-of-thought prompting elicits reasoning in large language models”. In: *NeurIPS*. 2022.

[125] C. Wendler. *wendlerc/RenderedText*. 2023.

[126] H. Wu et al. “Q-instruct: Improving low-level visual abilities for multi-modality foundation models”. In: *arXiv preprint arXiv:2311.06783* (2023).

[127] P. Wu and S. Xie. “V*: Guided Visual Search as a Core Mechanism in Multimodal LLMs”. In: *CVPR*. 2024.

[128] xAI. *grok*. 2024.

[129] H. Xu et al. “Demystifying clip data”. In: *ICLR*. 2024.

[130] A. Young et al. “Yi: Open foundation models by 01. ai”. In: *arXiv preprint arXiv:2403.04652* (2024).

[131] L. Yu et al. *Modeling Context in Referring Expressions*. 2016. arXiv: `1608.00272 [cs.CV]`.

[132] T. Yu et al. “Rlhf-v: Towards trustworthy mllms via behavior alignment from fine-grained correctional human feedback”. In: *arXiv preprint arXiv:2312.00849* (2023).

[133] X. Yue et al. “Mammoth: Building math generalist models through hybrid instruction tuning”. In: *ICLR*. 2024.

[134] X. Yue et al. “Mmmu: A massive multi-discipline multimodal understanding and reasoning benchmark for expert agi”. In: *CVPR*. 2024.

[135] M. Yuksekgonul et al. “When and why vision-language models behave like bags-of-words, and what to do about it?” In: *ICLR*. 2022.

[136] X. Zhai et al. “Sigmoid loss for language image pre-training”. In: *ICCV*. 2023.

[137] Y. Zhai et al. “Fine-Tuning Large Vision-Language Models as Decision-Making Agents via Reinforcement Learning”. In: *arXiv preprint arXiv:2405.10292* (2024).

[138] Y. Zhai et al. “Investigating the catastrophic forgetting in multimodal large language models”. In: *CPAL*. 2024.

[139] C. Zhang et al. “Raven: A dataset for relational and analogical visual reasoning”. In: *CVPR*. 2019.

[140] Y. Zhang et al. “Llavar: Enhanced visual instruction tuning for text-rich image understanding”. In: *arXiv preprint arXiv:2306.17107* (2023).

[141] Y. Zhao et al. “Pytorch fsdp: experiences on scaling fully sharded data parallel”. In: *arXiv preprint arXiv:2304.11277* (2023).

[142] L. Zheng et al. “Judging llm-as-a-judge with mt-bench and chatbot arena”. In: *NeurIPS*. 2024.

[143] T. Zheng et al. “OpenCodeInterpreter: Integrating Code Generation with Execution and Refinement”. In: *arXiv preprint arXiv:2402.14658* (2024).

[144] V. Zhong, C. Xiong, and R. Socher. “Seq2sql: Generating structured queries from natural language using reinforcement learning”. In: 2017.

[145] B. Zhou et al. "Semantic understanding of scenes through the ade20k dataset". In: *IJCV* (2019).

[146] K. Zhou et al. "Don't Make Your LLM an Evaluation Benchmark Cheater". In: *arXiv preprint arXiv:2311.01964* (2023).

[147] B. Zhu et al. *Starling-7b: Improving llm helpfulness & harmlessness with rlaif*. 2023.

[148] F. Zhu et al. "TAT-QA: A question answering benchmark on a hybrid of tabular and textual content in finance". In: *ACL*. 2021.

[149] Y. Zhu et al. "Visual7w: Grounded question answering in images". In: *CVPR*. 2016.

A. Training, Infrastructure, and Implementation

All models in this paper were trained using TPU-V4 pods [53]; we evaluate using NVIDIA A6000, A100, and H100 cards. The experiments in Section 3.4 require less than 24 hours on a TPU-V4-128, while our final Cambrian-1 models are trained in less than 4 days on a TPU-V4-512.

To enable and facilitate large-scale parallel training on TPUs, we employ TorchXLA with FSDP [141] to handle training sharding and parallelism. Training a large-scale multimodal model with TorchXLA on TPU is a challenging journey, as there are no open-source codebases and many critical features are not supported in the TorchXLA or TorchXLA FSDP libraries. To provide a brief taste of the difficulties: TPUs require a static graph throughout the program, which requires ground-up rewrites of dynamically-written open-source PyTorch codebases; model resuming is not implemented in TorchXLA, which is especially crucial when training on preemptable TPUs; existing TorchXLA FSDP tutorials fail to compile due to version changes in TorchXLA, updates in Hugging Face Transformers & Accelerate, or simply inherent issues with the tutorial; loading very large models (over 30 billion parameters) with the TorchXLA FSDP library is natively impossible due to the 100GB memory constraints of TPU-V4s, and requires extensive workarounds.

To this end, we have rewritten or developed many new functions to make this research possible. For instance, we rewrote the TorchXLA FSDP Sharding API to load very large models; we implemented model resuming on TorchXLA; we rewrote parts of the Hugging Face Transformers FSDP and gradient checkpointing implementations to enable large-scale FSDP training. We are committed to open-sourcing our codebase and publishing a comprehensive tutorial to share our insights, with the hope of inspiring and supporting future research and open-source contributions to the TPU and TorchXLA ecosystem.

B. Analyzing the Benchmarks

MLLM Benchmark Performance Confusion Matrix

We evaluate the benchmark scores for our one-stage, two-stage finetune-only and hybrid models, and then plot the correlation matrix for the pool of MLLM benchmarks. The correlation plot displays in Fig. 15. The result demonstrates that MMMU is less correlated in measuring model performance to other benchmarks. Nonetheless, we acknowledge it is widely used and therefore cluster it into knowledge-based QAs based on the nature of their questions.

C. Cambrian Vision-Centric Benchmark (CV-Bench)

C.1. Curation Procedure

We provide an overview of the data curation process in Fig. 16, which is conducted in a semi-automatic manner. The procedure consists of two main steps:

First, using the original benchmarks and their associated ground truth annotations, we generate query and answer pairs. These pairs are tailored to specific tasks: 2D-related tasks with COCO and ADE20K datasets, and 3D-related tasks with Omni3D.

Second, after generating the query and answer pairs, we engage human experts to manually filter out any incorrect or ambiguous queries to enhance the quality of benchmark. Each query is assigned one of three statuses: accepted (used as is), modified (where the incorrect answer is modified), and rejected (queries that are ambiguous, such as those too small or difficult to discern, even for human experts).

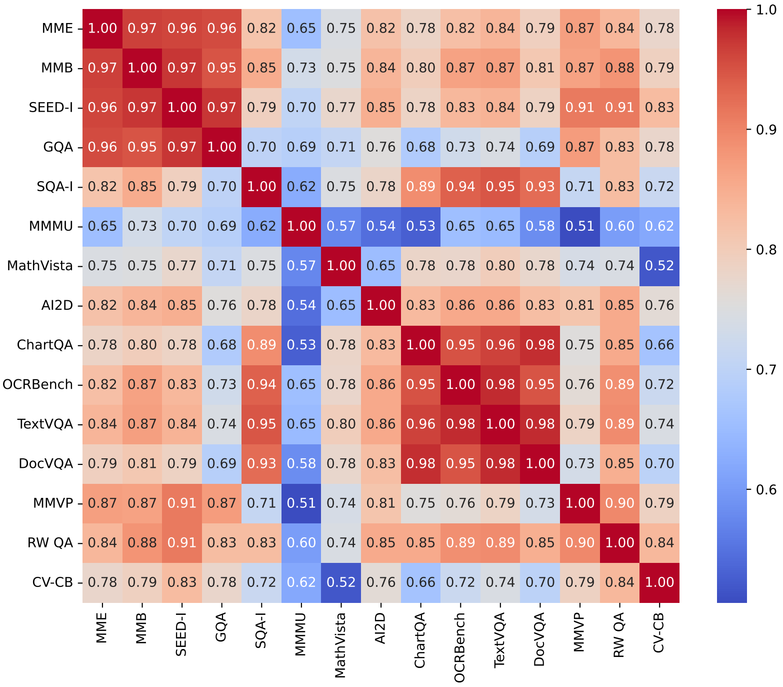

Figure 15 | **Correlation matrix for MLLM benchmarks.** The correlation matrix for MLLM benchmarks with respect to different vision backbones. The correlation matrix helps us to analysis and group benchmarks.

Following this two-stage process, we finalize the benchmark, which results in a total of 2638 image queries with improved accuracy and reliability. Subsequently, we will discuss the methods of human verification and the evaluation metrics used in this process.

C.2. Human verification

There are multiple reasons for the above generated data to be inaccurate. One of the main reasons is sparse annotations, but occasionally there could be wrong annotations as well.

Thus, we need manual inspection to change/remove these examples generated. Here are a few criteria we followed while manually filtering COCO and ADE20k data.

For **Counting** question types, if all instances of a category are not annotated, the ground truth would have lower count than the actual number of instances appearing in the image. In a few cases where the image distinctly has different countable instances of the object, we change the options/answer. In case the count is ambiguous, we reject the data sample altogether.

For **Relative Distance** question types without annotation, if the question is asked about two objects A and B and if there are two instances of a specific category (say A), the relative location of A w.r.t B can be have multiple correct answers. We reject the sample in this case. We also reject cases with clear incorrect annotations.

C.3. Benchmark Evaluation

To ensure that equal importance is given to both 2D and 3D tasks, we use an evaluation metric that is the average of the accuracies obtained from these tasks. Specifically, the overall performance is calculated as follows:

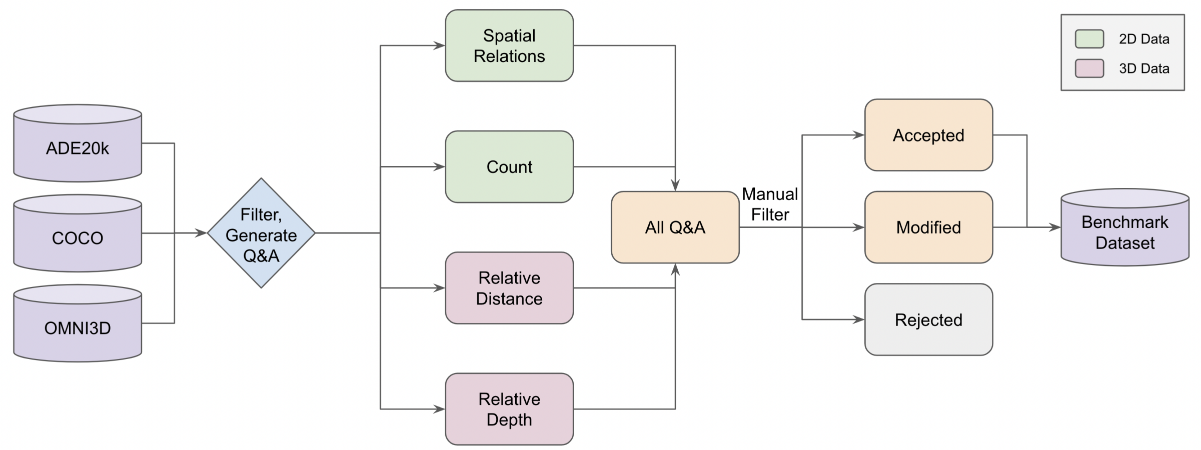

Figure 16 | **CV-CB Benchmark Filtering.** We reformulate classic 2D and 3D CV benchmarks into Q&A questions to evaluate MLLM's visual capabilities.

$$\text{Accuracy}_{2D} = \left(\frac{\text{Accuracy}_{COCO} + \text{Accuracy}_{ADE20k}}{2} \right)$$

$$\text{Overall Accuracy} = \left(\frac{\text{Accuracy}_{2D} + \text{Accuracy}_{3D}}{2} \right)$$

D. Vision Models in MLLMs

As mentioned in Section 3.4, we use MLLM as an interface to evaluate vision model's different capabilities. Here, we list details in terms of the model selection, full results, and data split.

D.1. Details of Vision Models

In our exploration of versatile vision models, we select thirteen models and group them into four categories: *language-supervised models* (i.e., OpenAI CLIP [102], SigLIP [136], DFN-CLIP [34], EVA-CLIP [113] and OpenCLIP [28]), *self-supervised models* (i.e., DINOv2 [96], I-JEPA [8], MAE [45], MoCo v3 [24]), *class-supervised models* (ImagetNet22K ViT [33]) and *other models* such as stable diffusion [104][7], segmentation models like SAM [61], and depth estimation models like MiDaS [13]. To provide a clear understanding of the specific variant evaluated, we meticulously detail their backbone architectures, resolution, number of tokens, and hidden dimension sizes in Table 9. For models that output a large number of patches in the last layer (e.g., SAM and ConvNeXt) we interpolate to the number of tokens specified in Table 9, and denote interpolation with $^{\text{I}}$.

D.2. Full Results of Different Vision Backbone in MLLM

For the above-listed vision models in Table 9, they are integrated as the vision encoder of the MLLMs. These MLLMs are trained on various adapter adapter data splits (i.e., 0, 0.5 and 1.2 million), and subsequently fine-tuned on a 737K instruction tuning dataset provided in LLaVA-1.5[73]. For the adapter data splits, the 0M split indicates that no initial adapter pertaining phase is employed for the MLLM. The 0.5M data split utilizes the 558K adapter data from LLaVA-1.5[73], while the 1.2M variant uses ShareGPT4V-PT dataset [22].

[7] We extract features following the practice in [11]

Supervision Type	Method	Architecture	Patch Size	Res.	# Tok.	Hidden Size
Language-Supervised						
Language	OpenAI CLIP	ViT-L	14	336	576	768
	DFN-CLIP	ViT-L	14	224	256	1024
	DFN-CLIP	ViT-H	14	378	729	1280
	EVA-CLIP-02	ViT-L	14	336	576	1024
	SigLIP	ViT-L	16	384	576	1024
	SigLIP	ViT-SO400M	14	384	729	1152
	OpenCLIP	ConvNeXT-L	-	512	^{I}576	1536
	OpenCLIP	ConvNeXT-L	-	1024	^{I}576	1536
	OpenCLIP	ConvNeXT-XXL	-	1024	^{I}576	3072
Self-Supervised						
Contrastive	DINOv2	ViT-L	14	336	576	1024
	DINOv2	ViT-L	14	518	^{I}576	1024
	MoCo v3	ViT-B	16	224	196	768
	MoCo v3	ViT-L	16	224	196	1024
Masked	MAE	ViT-L	16	224	196	1024
	MAE	ViT-H	14	224	256	1280
JEPA	I-JEPA	ViT-H	14	224	256	1280
Other						
Segmentation	SAM	ViT-L	16	1024	^{I}576	1024
	SAM	ViT-L	16	1024	^{I}576	1280
Depth	MiDaS 3.0	ViT-L	16	384	576	1024
	MiDaS 3.1	ViT-L	16	518	1024	1024
Diffusion	Stable Diffusion 2.1	VAE+UNet	16	512	1024	3520
Class Labels	SupViT	ViT-L	16	224	196	1024
	SupViT	ViT-H	14	224	256	1280

Table 9 | Catalog of all vision backbones tested. ^{I} denotes that the visual tokens have been interpolated down to the specified length.

0M Adapter Data + 737K Instruction Tuning Data As shown in Table 10, we provide 20 results for different variants of the above-mentioned thirteen vision backbones. Among them, language-supervised models show superior performance. Especially, OpenCLIP ConvNeXT-XXL@1024 model surpasses all other models on DocVQA with over 12%, indicating its potential to handle OCR-related benchmarks.

0.5M Adapter Data + 737K Instruction Finetune As shown in Table 11 and Table 10, the inclusion of an alignment stage with 0.5M data split results in a notable increase in performance for DFN-CLIP ViT-H/14@378, from 36.21 to 49.94. This substantial improvement highlights the value of the alignment stage for enhancing certain vision backbones, suggesting its importance in harnessing the full potential of vision models.

1.2M Adapter Data + 737K Instruction Finetune As we increase the amount of data in the alignment phase, we observe a consistent performance improvement for SigLIP ViT-SO400M/14@384 from 46.79 to 49.72 to 53.09 across 0M, 0.5M to 1.2M data splits as shown in Table 10, Table 11 and Table 12.

1.2M Adapter Data + 737K Instruction Finetune with *Unfrozen* Vision Model Here, we present the results of different vision models trained with 1.2m adapter data and 737K instruction tuning data in Appendix D.2. Comparing to Appendix G.2, we observe nearly all

Vision Backbone			General				Knowledge				OCR & Chart				Vision-Centric			
Model	Architecture	Average	MME^P	MMB	SEED^I	GQA	SQA^I	MMMU^V	MathVista^M	AI2D	ChartQA	OCRBench	TextVQA	DocVQA	MMVP	RealWorldQA	CV-Bench^{2D}	CV-Bench^{3D}
Language Supervised																		
OpenAI CLIP	ViT-L/14@336	48.37	1,419.43	61.45	59.85	62.26	69.87	34.50	27.80	59.82	33.73	31.70	55.39	28.00	11.33	53.46	56.44	57.40
DFN-CLIP	ViT-L/14@224	38.78	1,172.50	49.53	49.74	52.94	67.74	34.00	27.30	56.99	16.75	4.87	44.81	11.19	6.67	46.97	40.29	52.08
DFN-CLIP	ViT-H/14@378	36.79	1,091.76	41.28	44.32	50.48	65.54	33.65	26.50	56.76	15.56	2.70	43.41	10.15	4.67	47.06	39.07	52.91
EVA-CLIP-02	ViT-L/14@336	45.84	1,325.17	58.21	62.99	62.03	68.67	35.00	27.50	58.26	19.40	22.50	51.08	16.36	24.67	52.68	52.98	54.83
SigLIP	ViT-L/16@384	48.80	1,383.42	61.02	63.56	61.85	68.91	35.29	29.70	57.87	34.96	29.60	56.73	28.31	23.33	52.68	52.95	54.83
SigLIP	ViT-SO400M/14@384	47.57	1,376.75	58.76	60.59	60.92	69.01	34.40	26.50	58.35	30.72	28.60	55.10	28.31	19.33	50.71	52.33	58.67
OpenCLIP	ConvNeXt-L@512	47.38	1,404.01	57.62	61.90	60.34	69.06	33.90	29.10	58.39	28.04	25.20	55.45	28.41	24.00	54.12	53.46	48.91
OpenCLIP	ConvNeXt-L@1024	39.02	1,139.60	14.64	49.59	37.91	65.71	34.30	27.30	54.13	32.97	12.05	52.61	38.36	9.67	47.45	52.68	38.04
OpenCLIP	ConvNeXt-XXL@1024	41.83	1,219.47	48.00	49.88	55.09	66.14	35.69	27.60	56.67	16.92	5.00	46.90	40.98	16.00	47.32	43.40	52.75
Self Supervised																		
DINOv2	ViT-L/14@336	41.18	1,262.66	49.62	56.80	60.30	65.10	35.00	26.40	56.41	16.48	3.10	44.04	11.90	18.67	50.20	49.43	52.25
DINOv2	ViT-L/14@518	40.60	1,242.48	51.00	53.39	60.38	64.55	34.50	26.20	57.53	15.11	2.90	44.28	10.95	14.00	48.63	46.13	57.90
MoCo v3	ViT-B/16@224	34.94	966.45	36.77	33.00	47.35	62.96	32.80	26.20	55.05	16.04	2.60	43.81	10.31	6.67	45.36	39.03	52.83
MoCo v3	ViT-L/16@224	34.70	1010.18	34.64	41.71	47.46	64.70	33.70	26.30	55.05	16.24	2.70	42.60	10.39	4.00	45.36	44.67	35.16
MAE	ViT-L/16@224	37.69	1,114.07	42.30	35.93	55.20	63.51	34.60	26.00	56.10	16.11	2.70	43.63	10.83	14.00	44.80	45.81	55.75
MAE	ViT-H/14@224	38.58	1,083.35	41.15	50.99	55.30	64.90	34.10	26.00	56.49	15.63	3.20	43.98	11.00	12.00	46.30	47.18	54.90
I-JEPA	ViT-H/14@224	38.88	1,132.07	44.68	51.74	55.37	66.04	34.20	26.40	56.09	15.84	3.00	43.66	11.48	10.67	46.01	46.74	53.50
Other																		
SAM	ViT-L/16@1024	31.74	585.78	20.34	36.34	39.85	65.49	34.50	25.10	53.92	16.16	2.70	42.37	9.25	2.00	44.44	35.65	50.50
SAM	ViT-H/16@1024	32.37	648.96	22.30	36.31	40.52	65.20	34.10	26.00	54.44	15.56	2.40	42.39	8.75	2.00	45.36	34.83	55.25
MiDaS 3.0	ViT-L/16@384	35.65	981.36	38.57	40.93	49.04	63.41	31.80	25.70	54.72	16.36	2.60	43.19	11.24	6.67	44.97	38.78	53.40
MiDaS 3.1	ViT-L/16@518	35.44	983.34	34.79	40.20	48.53	64.60	33.90	25.00	55.18	15.64	2.60	42.76	12.08	6.66	43.66	39.63	52.58
Diffusion	SD2.1/16@512	36.59	1,044.28	37.71	42.00	48.38	64.55	33.40	25.70	56.99	15.56	3.10	43.14	10.40	9.33	45.88	44.68	52.40
SupViT	ViT-L/16@224	40.13	1,197.39	46.55	54.72	57.27	65.94	34.00	28.00	56.22	16.44	3.10	43.52	11.82	16.67	46.67	48.49	52.75
SupViT	ViT-H/14@224	37.45	1,082.43	42.61	48.45	52.98	63.51	35.29	26.50	55.78	15.16	3.30	44.16	11.49	4.66	43.79	44.55	52.91

Table 10 | **All Benchmark Results for 0M Adapter Data + 737K Instruction Tuning Data**

the models see improvement on most of the benchmarks, especially on the OCR & Chart and Vision-Centric benchmarks.

1.2M Adapter Data + 5M Instruction Finetune We present the results of 5M instruction tuning experiments in Fig. 7 here. In Table 13, we observe that after 5m instruction tuning, the gap between DINOv2 and CLIP models continue to bridge on general, knowledge and vision-centric benchmarks.

D.3. Model Ensemble

Model Ensemble Details We introduce the implementation details of the model ensemble in Section 3.5. For a given image, the image passes through each vision encoder to obtain the features from the last layer. The shape of each model's output differs depending on the resolution and patch size of each vision model. To resolve these differences, we interpolate the output of each model to a fixed number of tokens, using 576 tokens in our implementation, as described in Section 3.5. Our example code for interpolation can be seen below.

```
# Example code for interpolation
b, num_tokens, dim = image_features.shape
if num_tokens != self.image_token_len:
    target_h = target_w = int(np.sqrt(self.image_token_len))
    h = w = int(np.sqrt(num_tokens))
    image_features = image_features.view(b, h, w, dim)
    image_features = image_features.permute(0, 3, 1, 2).contiguous()
    image_features = F.interpolate(image_features), size=(target_h, target_w), mode=’bilinear’, align_corners=False)
    image_features = image_features.permute(0, 2, 3, 1).contiguous().flatten(1, 2)
```

We then concatenate the model outputs along the feature dimension and use a larger MLP to project the concatenated visual tokens into the LLM token space.

Vision Backbone			General				Knowledge				OCR & Chart				Vision-Centric			
Model	Architecture	Average	MME^{P}	MMB	SEED^{I}	GQA	SQA^{I}	MMMU^{V}	MathVista^{M}	AI2D	ChartQA	OCRBench	TextVQA	DocVQA	MMVP	RealWorldQA	CV-Bench^{2D}	CV-Bench^{3D}
Language-Supervised																		
OpenAI CLIP	ViT-L/14@336	49.03	1,413.51	60.34	62.17	60.81	69.76	36.49	29.90	58.48	36.80	30.20	57.63	30.98	21.33	51.63	52.57	54.75
DFN-CLIP	ViT-L/14@224	45.59	1,382.75	57.36	63.26	60.54	66.81	35.09	29.20	57.71	22.88	23.45	52.27	18.82	21.33	51.31	49.59	50.63
DFN-CLIP	ViT-H/14@378	50.62	1,500.45	62.64	66.44	62.53	70.75	35.69	30.30	58.78	39.20	29.80	56.98	31.39	29.33	53.59	54.96	52.58
EVA-CLIP-02	ViT-L/14@336	47.13	1,362.07	62.64	63.96	61.66	69.46	35.89	27.90	56.96	20.96	26.10	53.93	19.07	20.00	53.07	56.28	58.16
SigLIP	ViT-L/16@384	48.11	1,381.48	61.79	61.87	59.45	70.25	35.99	28.80	57.58	28.76	28.20	54.90	25.60	26.00	52.29	52.89	56.33
SigLIP	ViT-SO400M/14@384	50.41	1,327.79	62.13	63.92	61.31	70.38	36.99	30.00	59.52	40.08	33.20	60.37	36.58	22.00	53.99	55.59	54.08
OpenCLIP	ConvNeXt-L@512	48.01	1,366.85	59.66	62.89	61.31	68.77	36.99	28.50	59.29	27.88	28.50	57.57	29.48	16.00	53.20	53.81	55.91
OpenCLIP	ConvNeXt-L@1024	40.29	1,084.62	12.94	51.02	49.78	65.47	34.20	27.60	56.36	29.92	13.25	50.37	43.67	13.33	49.08	51.85	41.58
OpenCLIP	ConvNeXt-XXL@1024	50.45	1,405.65	57.96	63.58	62.41	68.02	34.30	29.40	59.62	42.96	26.20	61.82	42.67	28.67	55.16	49.92	54.16
Self-Supervised																		
DINOv2	ViT-L/14@336	42.64	1,283.95	54.64	59.03	60.19	66.39	35.29	25.70	58.03	16.00	3.20	45.39	11.79	20.00	50.59	53.51	58.33
MoCo v3	ViT-B/16@224	38.50	1,159.10	40.00	51.37	54.97	65.25	33.70	27.20	55.51	16.36	3.30	44.42	11.42	10.67	46.14	45.80	52.00
MoCo v3	ViT-L/16@224	37.71	1,074.13	41.19	49.46	53.61	63.66	33.70	27.40	55.83	17.04	3.40	43.84	11.98	8.00	46.27	48.69	45.59
MAE	ViT-L/16@224	39.99	1,138.35	44.60	54.91	56.69	65.64	36.19	27.90	56.48	17.20	3.20	44.45	12.42	14.00	47.32	48.83	53.08
I-JEPA	ViT-L/14@224	39.91	1,180.12	44.26	52.86	55.32	65.94	34.40	27.00	57.16	15.88	3.20	44.36	11.61	13.33	46.27	52.19	55.83
Other																		
SAM	ViT-H/16@1024	32.18	649.99	22.47	36.37	40.46	64.60	32.50	25.80	54.66	15.80	2.70	42.40	8.89	0.00	45.62	37.02	53.08
MiDaS 3.0	ViT-L/16@384	40.07	1,183.95	47.40	53.00	56.15	66.19	32.90	27.60	56.61	17.00	3.00	44.34	11.55	19.33	47.32	45.01	54.58
Diffusion	SD2.1/16@512	38.26	1,123.46	42.04	50.66	53.63	65.74	33.30	24.50	57.48	14.52	3.30	43.95	10.62	10.00	43.53	48.24	54.50
SupViT	ViT-L/16@224	39.66	1,186.88	48.43	54.28	56.35	65.49	33.00	28.10	57.16	17.56	2.80	44.92	12.23	12.67	47.06	43.59	51.67

Table 11 | **All Benchmark Results for 0.5M Adapter Data + 737K Instruction Tuning Data**

Full results on Model Ensemble We present all the benchmarks from the model ensemble experiment in Section 3.5 in Table 3. As discussed in Section 1 and Section 3.4, this comprehensive view of benchmarks provides a better understanding of the model's performance compared to simply averaging across benchmarks. Adding a vision-only SSL model enhances the MLLM's performance in vision-centric benchmarks while maintaining strong capabilities in other categories.

E. Data

E.1. Catalog of Visual Instruction Data

Here, we provide a comprehensive catalog of visual instruction datasets utilized in our study. The datasets are categorized based on their primary focus, including general conversation and VQA data, OCR-related data, counting data, knowledge-based data, and language-only data. Table 15 summarizes these datasets and their respective references.

E.2. Additional System Prompts used in Cambrian Data

As our Cambrian data includes instructions/questions and responses of different types and formats (e.g., Short response with a single word or regular response as a complete sentence), it is important to specify the required response format in the instruction prompt to avoid ambiguity and possible conflicts. Some of the datasets already include such prompts and we add proper prompts for the remaining datasets. The detailed response formatting prompts we additionally add are listed in Table 16.

E.3. Data Engine

Comprehensive Implementation Details of the Data Engine

The data engine is designed to generate instruction tuning data for knowledge-based fields, where previous works rarely covers and MLLMs are not reliable to distill for from. The data

Vision Backbone			General				Knowledge				OCR & Chart				Vision-Centric			
Model	Architecture	Average	MME^P	MMB	SEED^I	GQA	SQA^I	MMMU^V	MathVista^M	AI2D	ChartQA	OCRBench	TextVQA	DocVQA	MMVP	RealWorldQA	CV-Bench^{2D}	CV-Bench^{3D}
Language-Supervised																		
OpenAI CLIP	ViT-L/14@336	50.49	1,476.65	61.96	65.45	62.78	69.06	35.00	29.50	58.94	37.84	30.90	58.21	32.11	28.66	54.90	54.14	54.60
DFN-CLIP	ViT-L/14@224	46.01	1,341.14	56.68	63.74	60.75	66.96	33.80	28.65	57.04	23.32	23.20	52.85	18.97	26.67	51.44	52.91	52.08
DFN-CLIP	ViT-H/14@378	51.17	1,426.32	62.38	67.29	62.89	69.01	35.89	30.00	60.01	41.08	30.60	57.53	31.69	32.67	55.95	55.46	55.00
EVA-CLIP-02	ViT-L/14@336	49.71	1,449.78	64.00	67.53	63.60	69.91	35.49	28.40	59.16	24.76	27.10	55.39	21.63	34.67	55.69	57.83	57.75
SigLIP	ViT-L/16@384	50.87	1,424.20	59.40	65.48	62.56	68.67	35.99	29.70	59.29	40.52	33.50	59.59	35.20	28.00	53.33	55.42	56.08
SigLIP	ViT-SO400M/14@384	53.91	1,455.64	63.66	67.62	63.70	72.10	36.09	29.30	61.59	43.76	37.20	61.82	40.19	36.60	56.99	59.61	59.58
OpenCLIP	ConvNeXt-L@512	49.16	1,416.87	60.60	63.87	61.87	69.92	35.79	29.50	59.36	34.40	28.00	58.36	28.41	27.33	51.90	54.64	51.80
OpenCLIP	ConvNeXt-L@1024	51.00	1,392.92	58.21	65.47	62.89	67.43	34.90	29.90	59.13	46.08	25.50	62.14	44.13	26.67	55.29	53.57	55.08
OpenCLIP	ConvNeXt-XXL@1024	52.18	1,402.94	59.40	65.21	62.73	68.27	33.10	29.30	59.84	48.00	28.00	63.27	48.11	34.67	55.95	53.83	55.08
Self-Supervsied																		
DINOv2	ViT-L/14@336	41.85	1,190.81	51.83	56.90	60.38	66.04	34.20	27.40	56.41	16.44	3.30	45.12	11.79	21.33	49.67	53.91	55.33
MoCo v3	ViT-B/16@224	38.88	1,129.32	41.62	52.19	55.03	65.89	33.30	28.30	56.44	16.48	3.00	44.09	11.47	12.00	47.58	45.17	53.00
MoCo v3	ViT-L/16@224	37.07	1015.20	37.28	48.31	52.63	65.49	34.50	27.60	55.41	16.92	3.10	43.57	11.50	14.67	45.49	45.17	40.75
MAE	ViT-L/16@224	40.39	1,132.80	43.40	55.67	57.42	66.04	35.59	27.80	56.48	17.36	3.30	44.53	12.30	16.00	47.71	49.24	56.75
I-JEPA	ViT-H/14@224	40.27	1,207.88	45.79	54.51	56.15	65.29	34.40	27.10	56.19	16.20	3.20	43.45	11.58	18.00	45.88	49.57	56.58
Other																		
SAM	ViT-H/16@1024	32.54	682.81	23.32	36.16	40.32	65.20	33.20	26.50	54.21	15.68	2.50	41.76	8.98	1.33	46.80	37.66	52.90
MiDaS 3.0	ViT-L/16@384	39.15	1,132.18	46.21	51.75	55.57	66.30	33.70	26.70	56.06	17.08	3.10	43.65	11.66	15.30	45.75	44.44	52.58
Diffusion	SD2.1/16@512	39.51	1,168.52	40.00	53.80	55.33	64.60	35.00	26.10	57.16	15.36	3.10	44.23	11.06	18.67	47.32	48.04	53.90
Supervised	ViT-L/16@224	39.12	1,216.11	45.28	51.46	55.88	64.15	34.70	26.80	55.76	16.80	2.80	44.42	11.61	11.33	47.97	44.62	51.60

Table 12 | **All Benchmark Results for 1.2M Adapter Data + 737K Instruction Tuning Data**

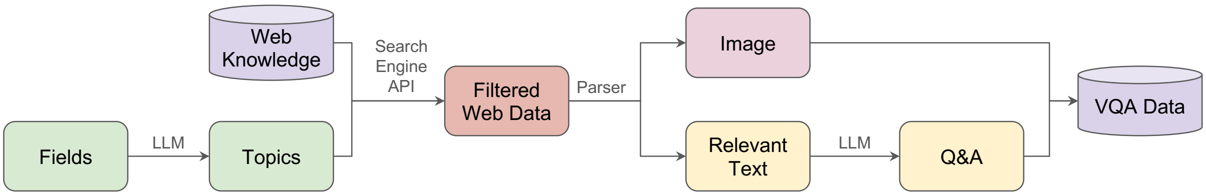

Figure 17 | **Targeted Internet Data Collection Engine.** We build a targeted internet data engine to collect high-quality and large-scale multimodal instruction tuning data for domains like knowledge.

engine takes in a given field, such as “Physics”, utilizing reliable web sources like Wikipedia. Below are the various stages involved in the process. We also visualize this process in Fig. 17:

Stage 1 - Topic Generation: We start by compiling a list of fields and subfields and subsequently generate topics for each field using a Large Language Model (LLM), such as GPT-4. In this stage, we processed 30 fields, resulting in 3660 topics. We then post-process the output of LLMs into json formats. For example, the topic data for Physics looks like below.

```
Physics
{
    "Classical Mechanics": [
        "Newton’s Laws of Motion",
        "Conservation of Energy",
        "Conservation of Momentum",
        "Harmonic Motion",
        "Rotational Dynamics",
        "Gravitation and Orbits",
        "Fluid Dynamics",
        "Elasticity and Plasticity",
        "Friction",
        "Waves and Sound",
        "Velocity and Acceleration",
        "Angular Momentum",
        "Statics and Equilibrium",
        "Kinematics of Particles",
        "Dynamics of Systems of Particles",
        "Collisions",
        "Centripetal Force and Acceleration",
        "Lagrangian and Hamiltonian Mechanics",
        "Chaos Theory",
        "Equations of Motion"
    ],
    "Electromagnetism": [
        "Coulomb’s Law",
        "Electric Field and Electric Potential",
        "Gauss’s Law",
        "Capacitance and Dielectrics",
        "Current and Resistance",
```

Vision Backbone			General				Knowledge				OCR & Chart				Vision-Centric			
Model	Architecture	Average	MME^{P}	MMB	SEED^{I}	GQA	SQA^{I}	MMMU^{V}	MathVista^{M}	AI2D	ChartQA	OCRBench	TextVQA	DocVQA	MMVP	RealWorldQA	CV-Bench^{2D}	CV-Bench^{3D}
Other																		
OpenAI CLIP	ViT-L/14@336	52.90	1,477.15	63.15	68.49	64.24	69.21	34.90	28.70	61.24	47.68	40.20	58.92	35.22	26.00	58.82	59.65	56.16
DFN-CLIP	ViT-L/14@224	45.80	1,364.91	55.15	63.06	59.94	67.28	35.59	29.80	58.65	20.48	23.40	52.23	18.29	22.67	50.85	53.59	53.50
EVA-CLIP-02	ViT-L/14@336	51.30	1,492.35	65.53	69.75	65.18	68.62	35.00	29.50	60.78	29.32	29.90	56.87	21.59	44.67	58.95	54.66	55.91
SigLIP	ViT-L/16@384	52.47	1,429.11	63.57	67.34	63.44	68.02	36.09	29.70	61.56	46.68	35.70	59.86	35.93	32.67	55.29	55.24	57.00
SigLIP	ViT-SO400M/14@384	55.27	1,489.05	66.55	69.59	64.58	70.45	35.69	29.20	62.34	51.28	40.80	63.28	43.02	38.00	59.61	61.58	53.91
OpenCLIP	ConvNeXt-L@512	52.76	1,467.38	63.40	66.92	63.17	69.16	34.90	29.70	58.45	52.04	35.40	61.87	38.79	30.67	56.21	54.24	55.91
Other																		
DINOv2	ViT-L/14@336	43.26	1,261.43	53.96	63.22	62.61	65.49	34.50	27.70	56.90	15.40	3.40	44.87	11.22	26.00	54.38	53.06	56.40
MoCo v3	ViT-B/16@224	39.51	1,175.34	41.70	53.31	56.15	65.25	33.40	28.30	55.76	15.48	3.20	44.42	11.10	18.00	46.67	45.38	55.25
MoCo v3	ViT-L/16@224	37.59	1075.39	39.15	50.14	53.65	65.49	34.60	27.30	55.44	17.28	3.00	44.21	11.70	14.67	44.58	45.38	41.12
MAE	ViT-L/16@224	41.43	1,181.51	45.53	58.92	58.75	64.65	35.00	29.20	57.12	16.88	3.10	44.67	11.74	18.67	49.67	53.04	56.83
I-JEPA	ViT-H/14@224	41.90	1,175.70	48.00	59.60	59.35	64.45	35.09	27.60	57.32	16.20	3.00	45.50	11.40	22.67	49.93	52.38	59.08
Other																		
MiDaS 3.0	ViT-L/16@384	38.28	1,065.26	42.64	50.95	56.10	65.39	35.00	27.20	52.98	15.96	2.80	43.49	11.23	12.00	46.14	43.41	53.90
Supervised	ViT-L/16@224	40.01	1,222.41	47.40	54.15	57.26	64.35	34.40	26.40	56.09	16.20	3.20	44.73	11.74	14.00	46.41	49.33	53.40

Table 13 | **All Benchmark Results for 1.2M Adapter Data + 737K Instruction Tuning Data with *Unfrozen* vision model**.

Vision Backbone				General				Knowledge				OCR & Chart				Vision-Centric			
Method	Backbone	Unfreeze	Average	MME^{P}	MMB	SEED^{I}	GQA	SQA^{I}	MMMU^{V}	MathVista^{M}	AI2D	ChartQA	OCRBench	TextVQA	DocVQA	MMVP	RealWorldQA	CV-Bench^{2D}	CV-Bench^{3D}
OpenAI CLIP	ViT-L/14@336	×	55.85	1,577.33	69.70	70.22	63.33	73.67	36.19	36.60	64.80	49.12	36.90	60.33	39.79	32.67	55.56	66.11	59.75
DINOv2	ViT-L/14@336	×	45.36	1,373.14	57.02	64.58	61.67	67.13	36.19	30.70	60.62	19.04	3.40	46.39	13.27	26.67	52.68	59.81	57.91
OpenAI CLIP	ViT-L/14@336	✓	57.44	1,585.34	68.68	71.47	63.96	77.39	36.09	37.30	65.12	59.36	48.00	62.39	45.24	31.33	56.21	61.09	56.16
DINOv2	ViT-L/14@336	✓	47.40	1,366.65	61.62	69.72	63.68	68.72	36.29	35.50	60.88	18.64	4.40	47.92	14.66	34.67	54.64	60.98	57.83

Table 14 | **All Benchmark Results for 1.2M Adapter Data + 5M Instruction Tuning Data**

```
        "Direct Current Circuits",
        "Magnetic Fields and Magnetic Forces",
        "Ampere’s Law",
        "Faraday’s Law of Induction",
        "Inductance",
        "Alternating Current Circuits",
        "Electromagnetic Waves",
        "Maxwell’s Equations",
        "Electromagnetic Radiation",
        "Optics and Light",
        "Quantum Electrodynamics",
        "Special Theory of Relativity Implication",
        "Magnetostatics",
        "Electrostatics",
        "Bioelectromagnetism"
    ],
    ...
}
```

Stage 2 - Filtering Web Data: For each generated topic, we utilize search engine APIs to fetch relevant high-quality web pages. For each topic, we query for 10 relevant links. Thus, we get 36,600 webpages post this stage. Here is an example of the data retrieved for the topic "Electric Field and Electric Potential":

```
"Electric Field and Electric Potential": [
    "https://en.wikipedia.org/wiki/Electric_potential",
    "https://en.wikipedia.org/wiki/Electric_field",
    "https://en.wikipedia.org/wiki/Electric_potential_energy",
    "https://en.wikipedia.org/wiki/Voltage",
    "https://en.wikipedia.org/wiki/Electricity",
    "https://en.wikipedia.org/wiki/Electrostatics",
    "https://en.wikipedia.org/wiki/Electric_dipole_moment",
    "https://en.wikipedia.org/wiki/Magnetic_vector_potential",
    "https://en.wikipedia.org/wiki/Electric-field_screening",
    "https://en.wikipedia.org/wiki/Electric_flux"
],
```

Stage 3 - Parsing: In this stage, we parse each web page to extract image-caption-text tuples. We aim to identify the blocks containing an image, the image’s caption, and relevant textual

Category	Datasets
General Conversation & VQA Data	LVIS-Instruct4V [122], SketchyVQA [120], OODVQA [120], VizWiz [44], ALLaVA [20], IDK [17], Q-Instruct [126], LAION GPT-4V [63], HatefulMemes [59], Visual7W [149], Visualmrc [114], AlfWorld [109], LNQA [101], LLaVA150K [75], ShareGPT [22], VQAv2 [43], GQA [50], OKVQA [88], A-OKVQA [108], RefCOCO [131], VisualGenome [62], GPT-4V recorded chat
OCR Related Data	LLAVAR [140], ChartQA [89], DocVQA [90], DVQA [54], ArxivQA [69], AI2D [58], ScreenQA [49], SynthDog [60], IconQA [82], WTQ [99], WikiSQL [144], FinQA [26], HiTab [27], TAT-QA [148], TabMWP [81], Chart2Text [55], VisText [115], InfoVQA [14], ST-VQA [15], Rendered-Text [125], OCRVQA [93], TextCaps [111], ShareGPTOCRData [22]
Counting Data	TallyQA [1], CLEVR [52]
Knowledge-Based Data	**Code:** Design2Code [110], WebSight [64], Datikz [12] **Math:** MathVision [123], Geo170K [37], TQA [4], Inter-GPS [83], RAVEN [139], GeomVerse [57] **Science:** ScienceQA [84], PathVQA [46]
Language Only Data	Dolly [30], MathInstruct [133], WizardCoder [86], OrcaMath [92], Open-CodeInterpreter [143], OpenOrca [71]

Table 15 | Visual Instruction-Tuning Data Catalog

content. Below is an example of the parsed data for the same topic, "Electric Field and Electric Potential":

```
  {
"Electric Field and Electric Potential",
[
  {
    "section":  "Electrostatics",
    "text":  "An electric potential at a point r in a static electric field E is given by the line integral where C is an arbitrary path from some fixed reference point to r; it is uniquely determined up to a constant...  The generalization of electric potential to this case is described in the section Generalization to electrodynamics.",
    "images":  [
      {
        "url":  https://upload.wikimedia.org/wikipedia/commons/thumb/1/1e/VFPt_plus_thumb_potential+contour.svg/142px-VFPt_plus_thumb_potential+contour.svg.png,
        "caption":  "Electric potential of separate positive and negative point charges shown as color range from magenta (+), through yellow (0), to cyan (-).  Circular contours are equipotential lines.  Electric field lines leave the positive charge and enter the negative charge."
      },
      {
        "url":  https://upload.wikimedia.org/wikipedia/commons/thumb/e/e0/VFPt_charges_plus_minus_potential+contour.svg/288px-VFPt_charges_plus_minus_potential+contour.svg.png,
        "caption":  "Electric potential in the vicinity of two opposite point charges."
      }
    ],
    "link":  https://en.wikipedia.org/wiki/Electric_potential,
    "title":  "Electric potential",
    "field":  "Physics",
    "subfield":  "Electromagnetism",
    "topic":  "Electric Field and Electric Potential"
  },
        ...
    ]
}
```

Stage 4 - Data Generation: We generate dataset in this stage, ensuring high quality. We first filter out data samples with *fewer than 50 words* in the text. Then, instead of downloading images directly from the links retrieved during web parsing, we download high-resolution images from the original sources. We then convert formats like SVG or GIF into a common standardized format, PNG.

Question-Answer pairs are generated by using LLM such as GPT-3.5 from the image metadata, caption, and contextual text. These Q&A pairs and the image form our VQA dataset. We generated 165k data samples. Here is an example of the generated data:

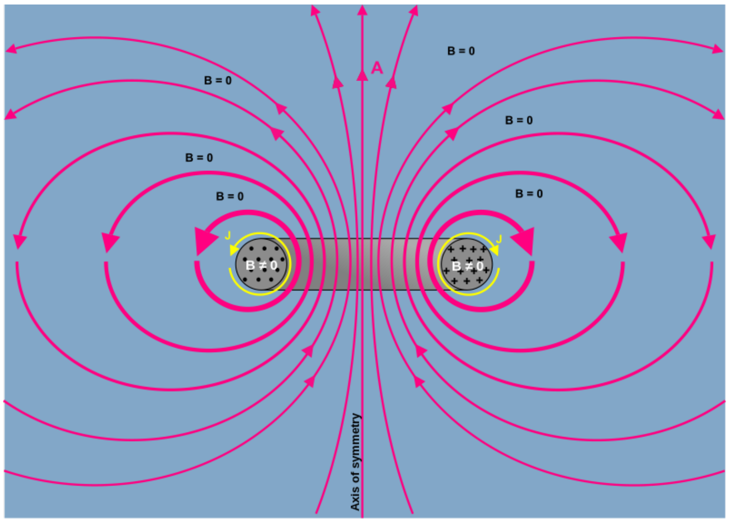

Figure 18 | **Dataset Image Id: `96232.png`**

```
 {
"id": "96232.png",
"image_id": "450px-Magnetic_Vector_Potential_Circular_Toroid",
"image_url": "...",
"text": "...",
"caption": "Representing the Coulomb gauge magnetic vector potential A, magnetic
flux density B, and current density J fields around a toroidal inductor of circular
cross section. Thicker lines indicate field lines of higher average intensity. Circles
in the cross section of the core represent the B-field coming out of the picture,
plus signs represent B-field going into the picture. \u2207 \u22c5 A = 0 has been
assumed",
"section": "Depiction of the A-field",
"...",
"Question": "What do the thicker lines signify?",
"Answer": "The thicker lines in the image represent paths of higher average
intensity in the magnetic vector potential A field. Shorter paths have higher intensity,
ensuring that the path integral remains constant. These lines are drawn to visually
convey the general behavior and intensity distribution of the A-field around the
toroidal inductor"
}
```

This data engine is designed for scalability and efficiency and is capable of handling extensive data generation tasks using multithreading techniques.

E.4. Full results on data curation experiment

Data Balance via Fitlering *t* As discussed in Section 5.2, if left unfiltered, the data pool is dominated by noisy, unbalanced data sources such as CLEVR and DVQA, leading to pronounced exponential tails. However, as we apply different t values to filter data from each source, the exponential tails become less pronounced, resulting in a more balanced dataset. We also present all the results in Table 17. t value 250k has the highest average across all benchmarks; 250k and 350k also have the highest performance across many individual benchmarks.

Data Ratio Studies We present the full results of our data ratio study in Table 18. The table highlights the importance of finding an optimal data ratio that balances different aspects of MLLM. Experiment 5 achieves well-rounded performance with its selected data ratio.

E.5. 737K and 5M Mixes

0.7M For the 0.7M data we used in Section 3.4, We add a small number of OCR and chart data to LLaVA 665K, specifically 15,501 AI2D, 14,999 DocVQA, and 13,000 DVQA data points. This results in a 737K mix, which covers all categories in training MLLMs. This data mix allows us to study visual representations efficiently.

5.0M For the 5M data mixes we use in Section 3.4, we apply data filtering discussed in Section 5.2 and apply t=150k on all multimodal instruction data in Cambrian-10M.

F. Implementation Details

Cambrian Models. For our final Cambrian models, we use 2.5M adapter data which is comprised of 1.2M captioning data from shareGPT4V [22] and 1.2M captioning data used in MiniGemini [70].

SVA. We introduce learnable $k_m \times k_m$ positional encodings in the vision features when $k_m > 1$. Besides, during cross-attention, the query is augmented with a global feature obtained by global pooling over the vision features, which is concatenated with $\mathbf{q}_{i,j}$ to better guide the aggregation process. In our experiments, the feature maps of all vision encoders except for ConvNext are interpolated to 576×576 ($m_k = 1$ for $L = 24$). For ConvNext, we first interpolate the feature maps from its 4 stages to 96×96 ($m_k = 4$ for $L = 24$) and then channel-wise concatenate them to form its final vision feature map similar to [70].

For experiments in Section 4, we set $D = 3$, $G = 1$ and add cross-attention layers between the layers of LLM with a stride equal to 3. For our final Cambrian models, we set $D = 3$, $G = 1$ and insert multiple cross-attention layers in LLM considering the tradeoff between performance and efficiency. For Cambrian-8B, Cambrian-13B, and Cambrian-34B, the strides of cross-attention layers inside the LLM are 3, 4, and 9 respectively.

G. Evaluation Details

G.1. System Prompts Used in Evaluation

To ensure the reproduction of our results, we also include the system prompts we used in this work. The system prompts for our models can be found in Table 21. Additionally, we release the prompts we used while evaluating our models on the various benchmarks in Table 22. We hope this sets a precedent for future research to improve the reproducibility of benchmark results.

G.2. Ablation Study on Fuzzy Matching Vs LLM Judgement

We use fuzzy matching to evaluate responses in some benchmarks, since MLLMs can answer questions with auxillary phrases. To study the effectiveness of our fuzzy matching, we compare our model accuracy through fuzzy matching with the model accuracy obtained when we use LLM as a grader.

The LLM grader is sensitive to the prompt given to it while grading, and we prompt the LLM (we use OpenAI GPT-3.5-turbo and GPT-4-turbo as our graders) with few shot grading examples, which we notice significantly improves grading accuracy. An example of such a prompt is given below.

LLM Grader Prompt

```
You are a reliable grader. Reply with only either of the following
2 words: CORRECT or INCORRECT.
You will be given an ’answer’ and a ’gt_answer’ (ground truth answer)
,and you must reply with either CORRECT or INCORRECT based on the
response. Tolerate a 0.05 relative error for numerical answers.
answer: 25
gt_answer: 29
evaluation: INCORRECT
answer: Yes
gt_answer: Yes
evaluation: CORRECT
answer: 80
gt_answer: 80
evaluation: CORRECT
answer: Ireland
gt_answer: Italy
evaluation: INCORRECT
answer: UK
gt_answer: UK
evaluation: CORRECT
answer: 2019
gt_answer: 2011
evaluation: INCORRECT
answer: {answer}
gt_answer: {gt_answer}
evaluation:
```

We conduct an ablation study on the benchmarks that require fuzzy matching and present the results in Table 20. We discover that fuzzy matching provides reliable results compared to an LLM grader. We recommend using a more capable model (such as GPT-4-turbo) for grading benchmarks that have more subjective responses (such as numbers and words).

Index	Response formatting prompts
1	Answer the question using a single word or phrase.
2	Answer the question using a single number or phrase.
3	Answer with the option's letter from the given choices directly.
4	Give the short answer directly.
5	Answer the question using a single word or phrase.
6	When the provided information is insufficient, respond with <no answer>.
7	Directly provide the HTML code.
8	First show your reasoning process and then give the final answer.
9	When the provided information is insufficient, respond with 'Unanswerable'. Answer the question using a single word or phrase.
10	Answer with the letter.

Dataset	Prompts added
SketchyVQA	1
OODVQA	1
VizWiz	9
Q-Instruct	1, 3
ChartQA	2
DocVQA	4
DVQA	1
AI2D	1
ScreenQA	1, 6
CLEVR	1
TallyQA	1
PathVQA	1
MathInstruct	8
Design2Code	7
IconQA	1, 10
HiTab	1
WTQ	1
WikiSQL	1
Inter-GPS	10
Visual7W	3
TQA	10
RAVEN	1

Table 16 | Response formatting prompts for Cambrian Data

			General				Knowledge				OCR & Chart				Vision-Centric			
	# of Data	Average	MME^{P}	MMB	SEED^{I}	GQA	SQA^{I}	MMMU^{V}	MathVista^{M}	AI2D	ChartQA	OCRBench	TextVQA	DocVQA	MMVP	RealWorldQA	CV-Bench^{2D}	CV-Bench^{3D}
$t = 150k$	4015k	53.74	1,512.3	67.0	68.3	61.2	73.4	35.1	34.3	62.4	44.6	39.1	58.5	38.5	30.0	55.2	61.98	54.7
$t = 250k$	5218k	54.31	1,475.9	67.3	69.2	61.6	73.4	35.9	34.5	62.4	46.5	36.9	59.2	38.6	32.0	56.6	63.68	57.5
$t = 350k$	5883k	54.27	1,461.9	66.2	68.9	61.6	73.8	36.4	32.8	62.5	46.8	38.3	59.3	39.3	31.3	54.9	62.68	60.4
$t = 450k$	6383k	54.15	1,534.1	67.6	66.3	61.9	72.9	35.1	36.9	63.8	45.8	38.6	58.4	39.4	28.0	53.6	64.60	56.8

Table 17 | **All Benchmark Results for Data Balancing Experiments**

	General					Knowledge				OCR & Chart				Vision-Centric			
	Average	MME^{P}	MMB	SEED^{I}	GQA	SQA^{I}	MMMU^{V}	MathVista^{M}	AI2D	ChartQA	OCRBench	TextVQA	DocVQA	MMVP	RealworldQA	CV-Bench^{2D}	CV-Bench^{3D}
exp1	47.49	1,309.10	58.00	60.10	54.00	72.40	34.80	31.20	59.10	34.20	34.50	54.20	33.00	13.30	47.60	57.40	50.58
exp2	47.78	1,351.70	60.30	61.20	55.40	72.80	35.20	29.50	59.10	31.20	33.40	54.20	30.50	15.30	48.20	58.40	52.25
exp3	48.28	1,299.53	60.56	61.79	55.74	72.04	34.90	32.10	59.40	33.20	33.90	54.15	31.90	21.30	48.60	58.52	49.41
exp4	47.47	1,288.98	58.16	61.47	55.00	71.05	37.10	28.20	58.50	33.72	34.50	55.07	31.69	20.66	47.06	56.30	46.58
exp5	48.96	1,363.26	60.48	63.18	55.92	70.35	35.70	31.40	57.19	32.88	34.60	54.74	32.10	22.70	47.30	58.83	57.75

Table 18 | **All Benchmark Results for Data Ratio Experiments with fixed 1350k data**

	Backbone		Data		Adapter			Instruction Tuning			
Experiment	LLM	Vision	Adapter	Instruction Tuning	lr	wd	bs	lr	wd	bs	vision lr
0M Adapter+737K IT	Vicuna-1.5-7B	OpenAI CLIP ViT-L/14@336	0	737k	-	-	-	2e-5	0	512	-
0.5M Adapter+737K IT	Vicuna-1.5-7B	OpenAI CLIP ViT-L/14@336	0.5M	737k	1e-3	0	512	2e-5	0	512	-
1.2M Adapter+737K IT	Vicuna-1.5-7B	OpenAI CLIP ViT-L/14@336	1.2M	737k	1e-3	0	512	2e-5	0	512	-
Unfreeze Vision	Vicuna-1.5-7B	OpenAI CLIP ViT-L/14@336	1.2M	737k	1e-3	0	512	2e-5	0	512	1e-5
Model Ensemble	Vicuna-1.5-7B	Chosen Combination	1.2M	737k	1e-3	0	512	2e-5	0	512	
Data Balance	Vicuna-1.5-7B	OpenAI CLIP ViT-L/14@336	0	Mix Based on three *t*	-	-	-	2e-5	0	512	-
Data Ratio	Vicuna-1.5-7B	OpenAI CLIP ViT-L/14@336	0	1350k Based on Ratio	-	-	-	2e-5	0	512	-
LLaVA 665K	Vicuna-1.5-7B	OpenAI CLIP ViT-L/14@336	0	LLaVA 665K	-	-	-	2e-5	0	512	-
Cambrian-10M (Data)	Vicuna-1.5-7B	OpenAI CLIP ViT-L/14@336	0	Cambrian-10M	-	-	-	2e-5	0	512	-
Cambrian-7M (Data)	Vicuna-1.5-7B	OpenAI CLIP ViT-L/14@336	0	Cambrian-7M	-	-	-	2e-5	0	512	-
Cambrian-1-8B	Llama-3-Ins-8B	SVA with 4 encoders*	2.5M	Cambrian-7M	1e-4	0	512	2e-5	0	512	-
Cambrian-1-13B	Vicuna-1.5-13B	SVA with 4 encoders*	2.5M	Cambrian-7M	1e-4	0	512	2e-5	0	512	-
Cambrian-1-34B	Hermes-2-Yi-34B	SVA with 4 encoders*	2.5M	Cambrian-7M	1e-4	0	512	2e-5	0	1024	-

Table 19 | **Implementation details and hyperparameters for all experiments.** *4 encoders are: OpenAI CLIP ViT-L/14@336, SigLIP ViT-SO400M/14@384, DINOv2 ViT-L/14@518, OpenCLIP ConvNeXt-XXL@1024

Method	Eval	SEED^{I}	GQA	SQA^{I}	MMMU	AI2D	ChartQA	OCRBench	TextVQA	MMVP	RealWorldQA
Cambrian-1 8B	Fuzzy Matching	74.7	64.6	80.4	42.7	73.0	73.3	62.4	71.7	51.3	64.2
Cambrian-1 8B	GPT3.5 Grading	78.4	65.8	82.0	38.9	78.1	71.2	67.0	69.2	49.3	63.5
Δ		+3.7	+1.2	+1.6	-3.8	+5.1	-2.1	+4.6	-2.5	-2.0	-0.7
Cambrian-1 13B	Fuzzy Matching	74.7	64.6	80.4	40.4	73.0	73.3	62.4	71.7	51.3	64.2
Cambrian-1 13B	GPT3.5 Grading	77.3	64.7	81.3	37.2	78.2	71.4	67.1	75.6	46.0	64.3
Δ		+2.9	+0.4	+2.0	-3.2	+4.6	-2.4	+5.2	+2.8	+4.7	+1.3

Table 20 | **Comparison between Fuzzy Matching Accuracy and LLM Judged Accuracy.** Fuzzy matching and LLM referee yield similar accuracies for the benchmarks that require matching.

LLM Backbone	System Prompt
Vicuna 1.5 7B	A chat between a curious user and an artificial intelligence assistant. The assistant gives helpful, detailed, and polite answers to the user's questions.
LLAMA-3 8B	You are Cambrian, a highly intelligent multimodal AI trained by NYU Vision X. As a multimodal AI, you have the ability to process and analyze images. Whenever an image is present in the conversation, very carefully examine it and consider its content when formulating your response.You should give concise responses to very simple questions, but provide thorough responses to more complex and open-ended questions.
Nous-Yi 34B	You are Cambrian, a highly intelligent multimodal AI trained by NYU Vision X. As a multimodal AI, you have the ability to process and analyze images. Whenever an image is present in the conversation, very carefully examine it and consider its content when formulating your response. You should give concise responses to very simple questions, but provide thorough responses to more complex and open-ended questions.

Table 21 | LLM Backbone System Prompts

Table 22 | Listing the prompts used in the evaluation of each benchmark

Benchmark	Prompt	Example
AI2D	\nAnswer with the option's letter from the given choices directly.	USER: <image>\nwhich of these define dairy item\n(A) c\n(B) D\n(C) b\n(D) a\nAnswer with the option's letter from the given choices directly. ASSISTANT:
ChartQA	\nAnswer the question using a single number or phrase.	USER: <image>\nHow many food item is shown in the bar graph?\nAnswer the question using a single number or phrase. ASSISTANT:
DocVQA	\nGive the short answer directly.	USER: <image>\nWhat is the dividend payout in 2012?\nGive the short answer directly. ASSISTANT:
GQA	\nAnswer the question using single word or phrase.	USER: <image>\nIs it overcast?\nAnswer the question using single word or phrase. ASSISTANT:
MathVista	\nFirst show your reasoning process and then give the final answer.	USER: <image>\nwhat is the total volume of the measuring cup?\nFirst show your reasoning process and then give the final answer. ASSISTANT:
MM-Bench EN	\nAnswer with the option's letter from the given choices directly.	USER: <image>\nWhich of the following was a dependent variable in this experiment?\n(A) cocoon\n(B) chrysalis\n(C) nan\n(D) nan\nAnswer with the option's letter from the given choices directly. ASSISTANT:
MME	\nPlease answer the question using a single word or phrase.	USER: <image>\nIs a python code shown in the picture? Please answer yes or no.\nAnswer the question using a single word or phrase. ASSISTANT:
MMMU	\nAnswer with the option's letter from the given choices directly.	USER: <image>\nWhat causes these unusual formations on Mountain papaya? Options:\nA. Abiotic\nB. Confused\nC. Biotic\nD. Normal\nAnswer with the option's letter from the given choices directly. ASSISTANT:
MMVP	\nAnswer with the option's letter from the given choices directly.	USER: <image>\nAre the butterfly's wings closer to being open or closed? Options:\n(a) Open\n(b) Closed\nAnswer with the option's letter from the given choices directly. ASSISTANT:
OCR Bench	\nGive the short answer directly.	USER: <image>\nwhat is written in the image?\nGive the short answer directly. ASSISTANT:
RealWorld QA	\nAnswer the question using a single word or phrase.	USER: <image>\nIn which direction is the front wheel of the car on the right side facing?\n\nA. Left\nB. Straight\nC. Right\nAnswer the question using a single word or phrase. ASSISTANT:
SQA-I	\nAnswer with the option's letter from the given choices directly.	USER: <image>\nWhat is the name of the colony shown?\nA. Maryland\nB. New Hampshire\nC. Rhode Island\nD. Vermont\nAnswer with the option's letter from the given choices directly. ASSISTANT:

Benchmark	Prompt	Example
SEED-I	\nAnswer with the option's letter from the given choices directly.	USER: <image>\nHow many towels are in the image? Options:\nA. One\nB. Two\nC. Three\nD. Four\nAnswer with the option's letter from the given choices directly. ASSISTANT:
Text-VQA	\nAnswer the question using a single word or phrase.	USER: <image>\nwhat is the time?\nReference OCR tokens: N, u, g0\nAnswer the question using a single word or phrase. ASSISTANT:
ADE	\nAnswer with the option's letter from the given choices directly.	USER: <image>\nConsidering the relative positions of the cushion and the sofa in the image provided, where is the cushion located with respect to the sofa? Select from the following choices. \n(A) right\n(B) left\nAnswer with the option's letter from the given choices directly. ASSISTANT:
COCO	\nAnswer with the option's letter from the given choices directly.	USER: <image>\nHow many trains are in the image? Select from the following choices. \n(A) 3\n(B) 0 \n(C) 1 \n(D) 2 \n(E) 4\nAnswer with the option's letter from the given choices directly. ASSISTANT:
Omni3D	\nAnswer with the option's letter from the given choices directly.	USER: <image>\nEstimate the real-world distances between objects in this image. Which object is closer to the traffic cone (highlighted by a red box), the motorcycle (highlighted by a blue box) or the bus (highlighted by a green box)?\n(A) motorcycle\n(B) bus\nAnswer with the option's letter from the given choices directly. ASSISTANT: